Quantum Dynamics of Large Systems
Challenges and Possible Solutions

Eli Pollak
Chemical Physics Department
Weizmann Institute of Science
Rehovot, Israel
Eli.pollak@weizmann.ac.il

The challenges:

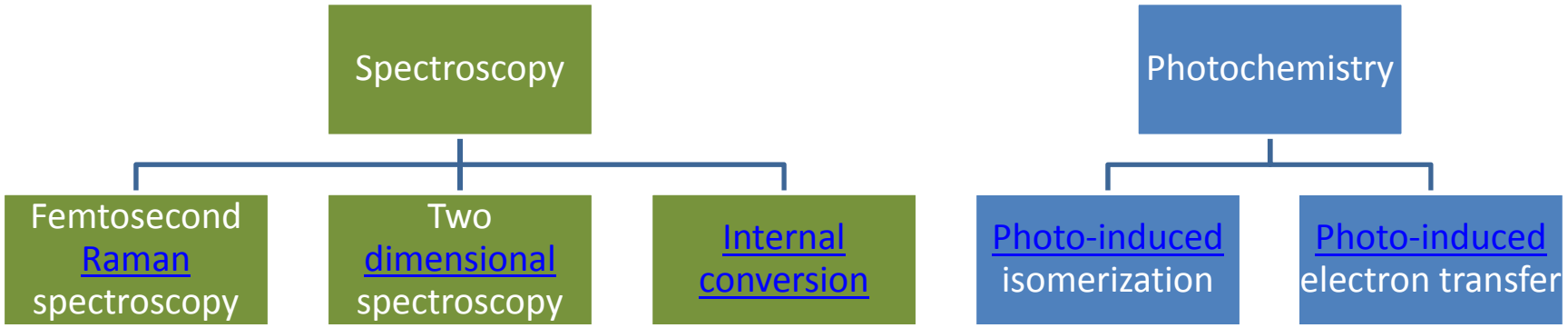

Femtosecond Raman spectroscopy

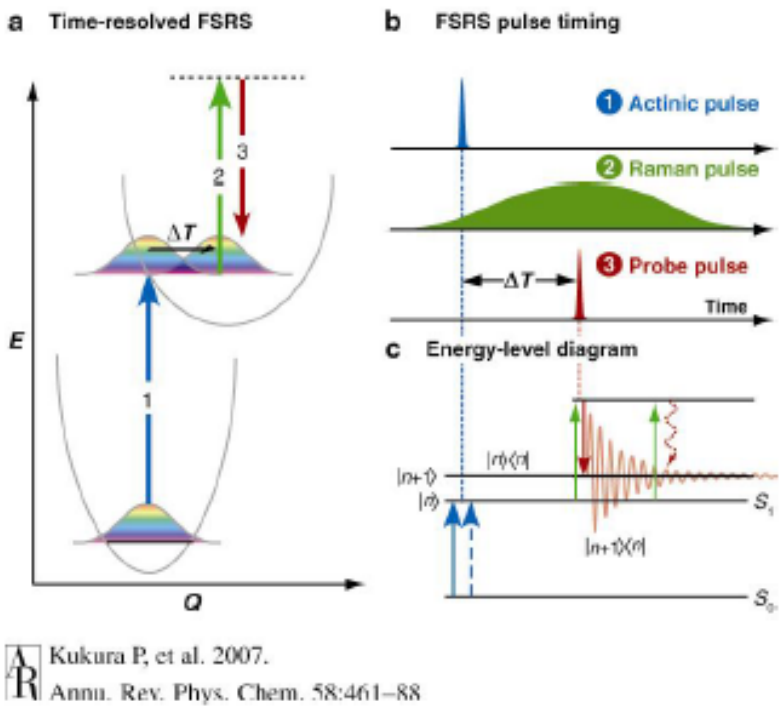

Figure 3 A femtosecond pump pulse (*1*) promotes the system to an excited electronic state. The evolution is then probed by Raman (*2*) and probe (*3*) pulses driving stimulated Raman transitions after a variable time delay, Δ*T*. (*c*) Bra-ket energy-level diagram illustrating the FSRS process. Solid and dashed arrows represent bra and ket electric-field couplings. At $t = 0$, two field couplings with the pump pulse promote the system to the excited state ($|n\rangle\langle n|$). After a specified time delay, Raman and probe pulses establish vibrational coherence on the excited state ($|n+1\rangle\langle n|$) with high temporal precision, which decays with the characteristic vibrational dephasing time. An additional field coupling with the long-duration electric field provided by the Raman pulse at any time during the vibrational free-induction decay results in the collinear emission of a Raman-shifted photon along the probe beam.

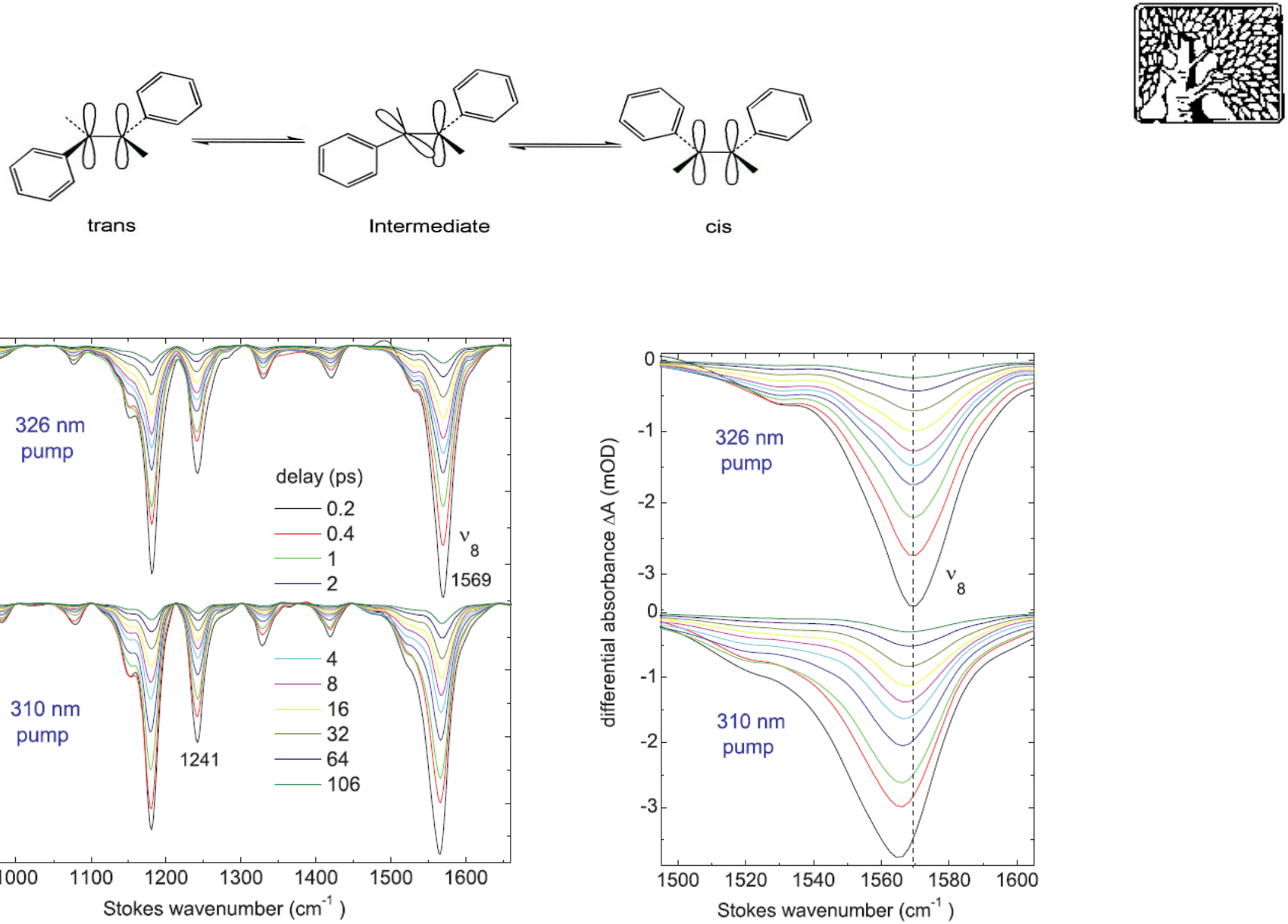

FIG. 3. FSR spectra from *trans*-stilbene in n-hexane upon pumping at 326 nm and 310 nm, in the range 960–1740 cm^{-1} (left), and around the ν_8 mode (right). The signal decays with $\tau \approx 80$ ps (20 °C) due to *trans-cis* isomerization. With 310 nm pumping the molecule is heated up initially by $\Delta T = 80$ K. Subsequent vibrational cooling causes a blueshift of the ν_8 band,[22] of 4 cm^{-1} in this case. With 326 nm pumping (zero excess energy) no shift is observed. If "excitation-induced cooling"[34] takes place, subsequent heating by the solvent would result in a 1 cm^{-1} redshift of the band per 20 K.

Photoinduced isomerization prototype

Isomerization of trans-stilbene in the electronically excited S_1 state:

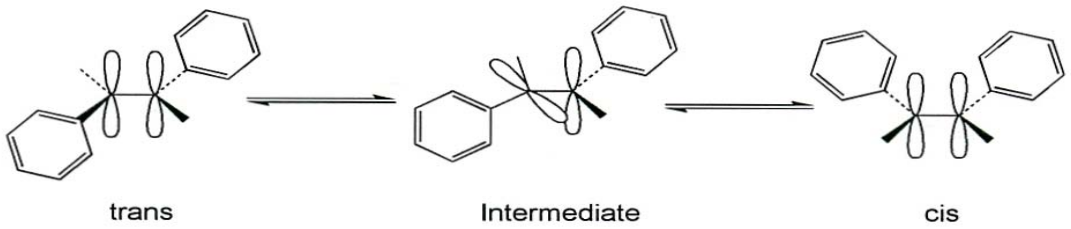

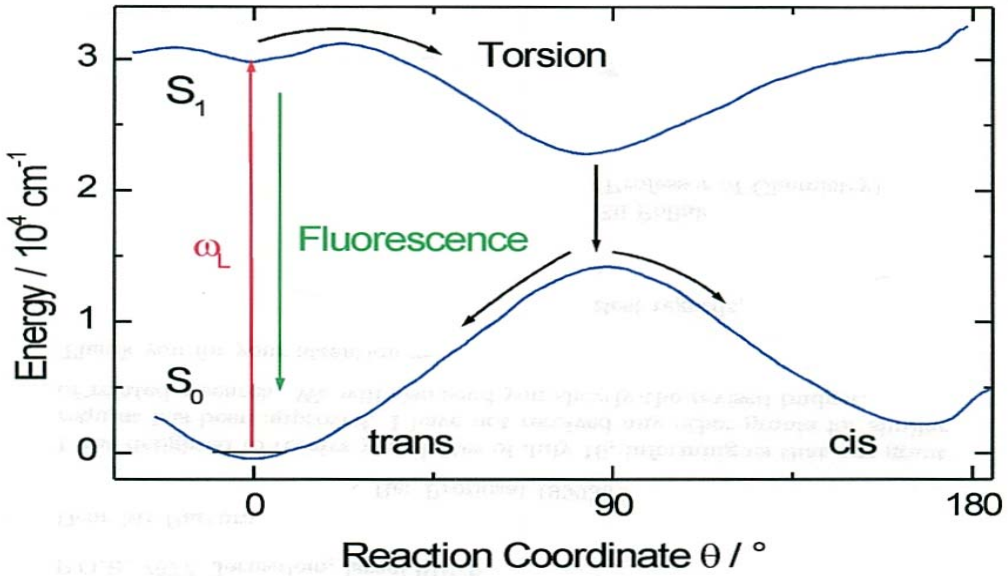

Raw data – fluorescence decay rates at different excitation wavelengths, adapted from Ch. Warmuth, F. Milota, H.F. Kauffmann, H. Wadi and E. Pollak, J. Chem. Phys. **112**, 3938 (2000).

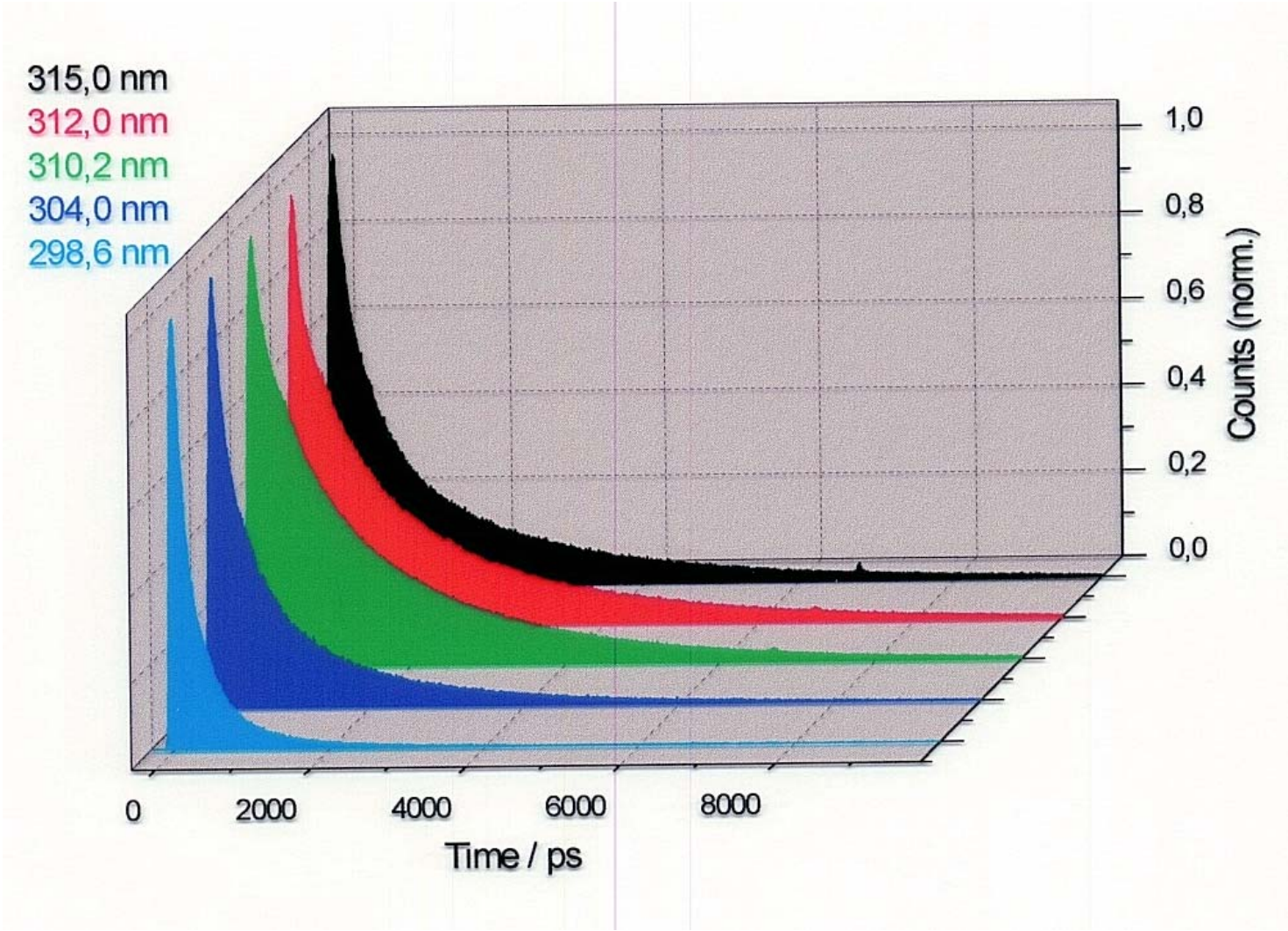

First step of vision – photo-isomerization of retinal

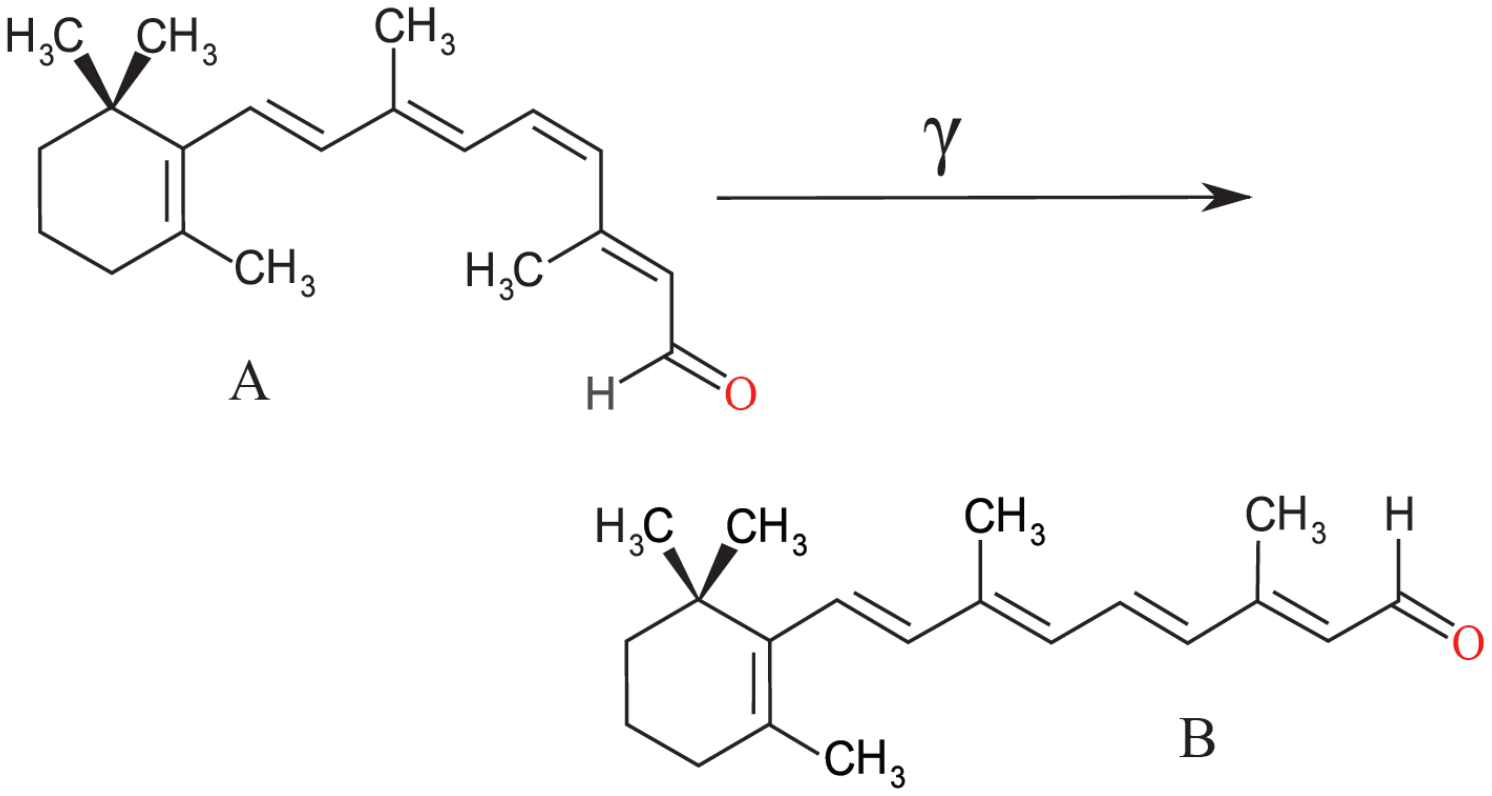

Photosynthetic Reaction Centers

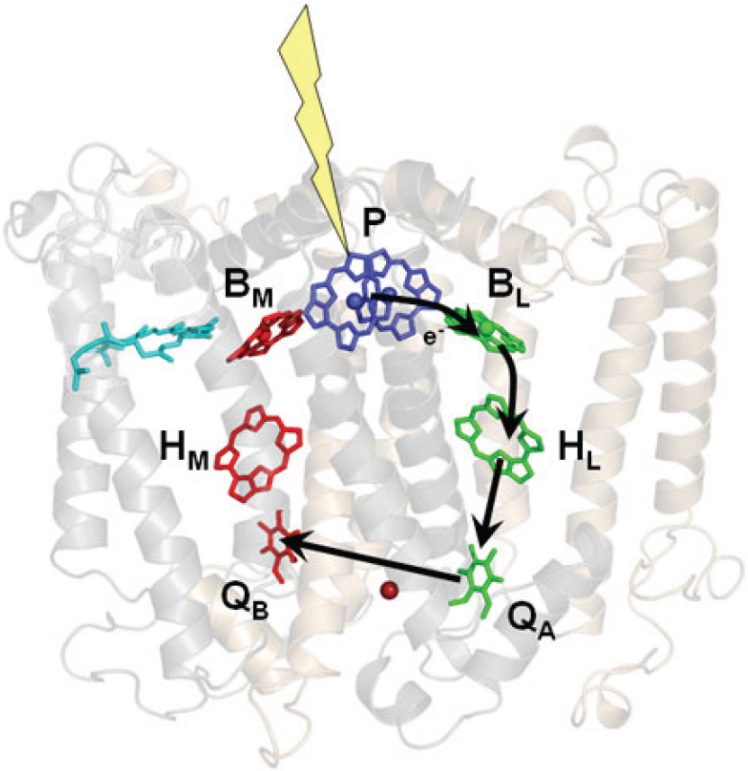

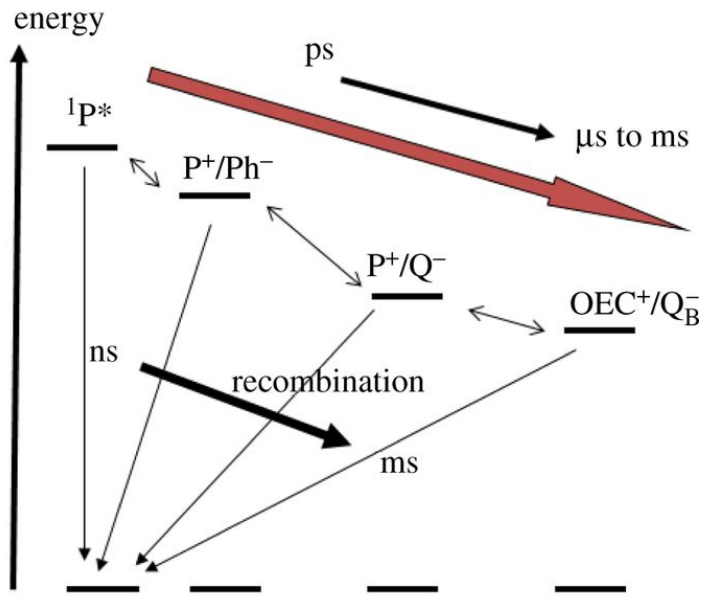

Nearly all known life relies on photosynthesis to convert solar energy into chemical energy, either directly or indirectly. The reaction center (RC) is the core where this conversion occurs. The bacterial RC consists of two branches of chromophores, which serve as electron shuttles. When excited, the special pair of bacteriochlorophylls (P) passes an electron to the bacteriopheophytin (H_L) in the active branch of chromophores in ~3 ps, with near unity quantum efficiency. The RC exhibits a high level of symmetry with two possible, seemingly equivalent, pathways for electron transfer. Nonetheless, electron transfer only occurs along one branch of chromophores, breaking the symmetry.

Two dimensional spectroscopy

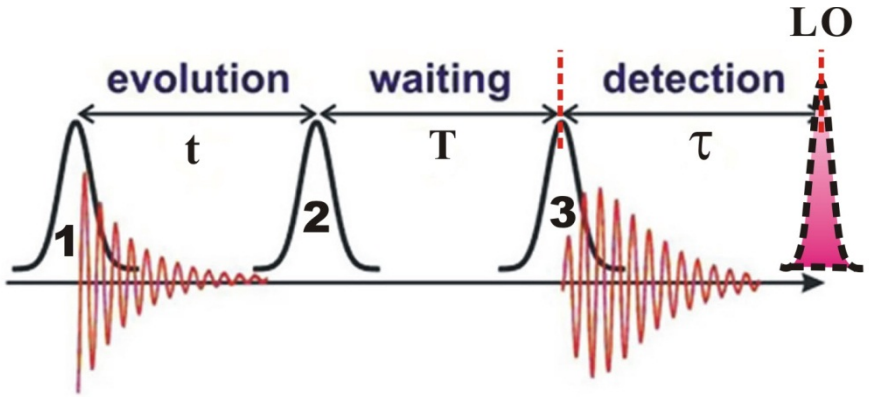

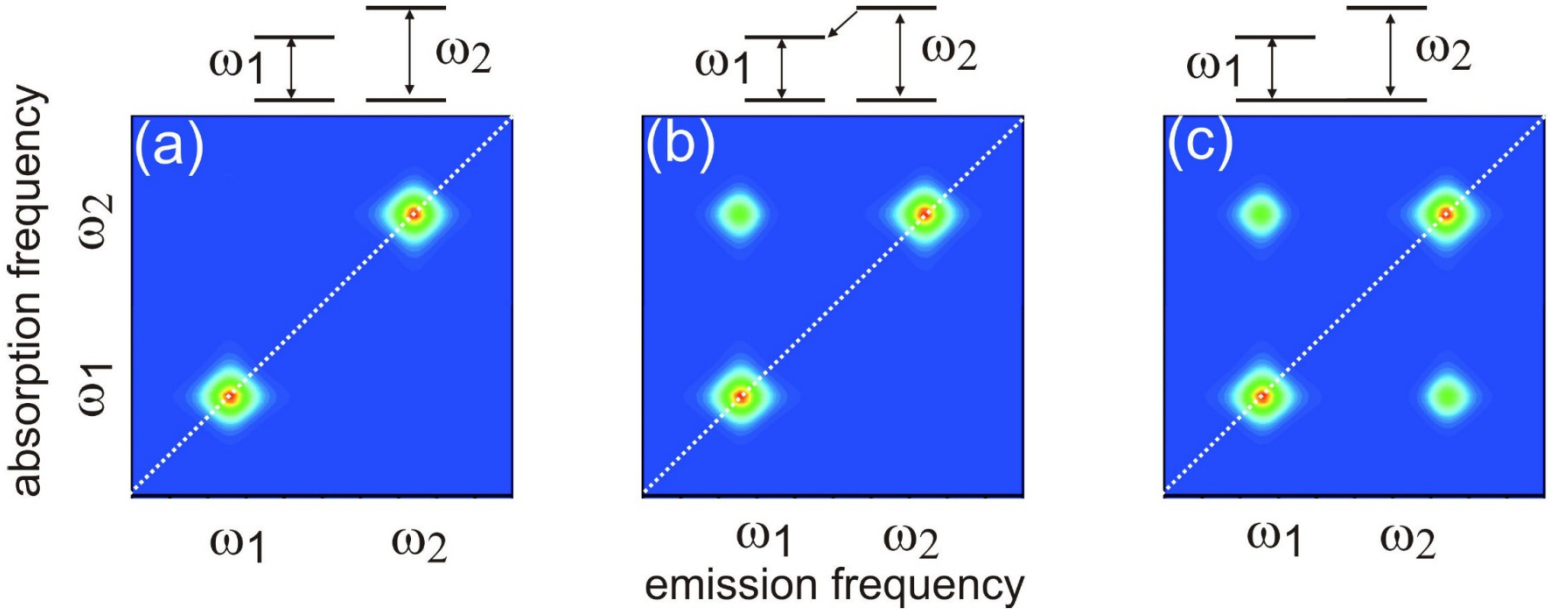

Figure 3: Time evolution of C2D spectra.

From

Dynamic localization of electronic excitation in photosynthetic complexes revealed with chiral two-dimensional spectroscopy

Andrew F. Fidler, Ved P. Singh, Phillip D. Long, Peter D. Dahlberg & Gregory S. Engel

Nature Communications **5**, Article number: 3286 doi:10.1038/ncomms4286

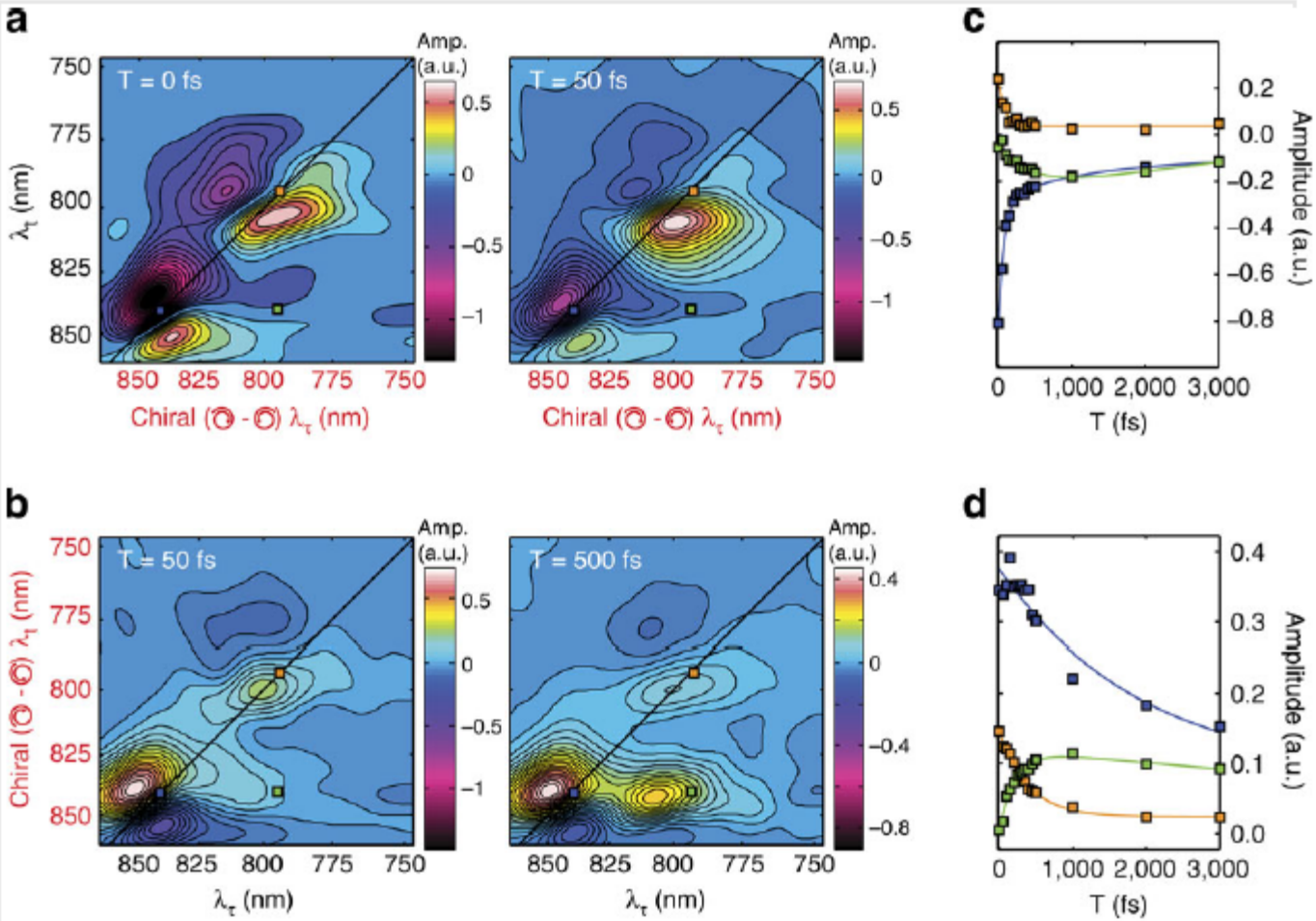

Chiral two-dimensional spectra for the indicated waiting times are shown for the chiral pump (**a**) and chiral probe (**b**). Traces through the two main features and the corresponding cross peak are shown in **c** and **d** for the chiral pump and chiral probe experiments, respectively. Fits of the traces to a sum of two exponentials are drawn as lines. Amp., amplitude.

Internal conversion

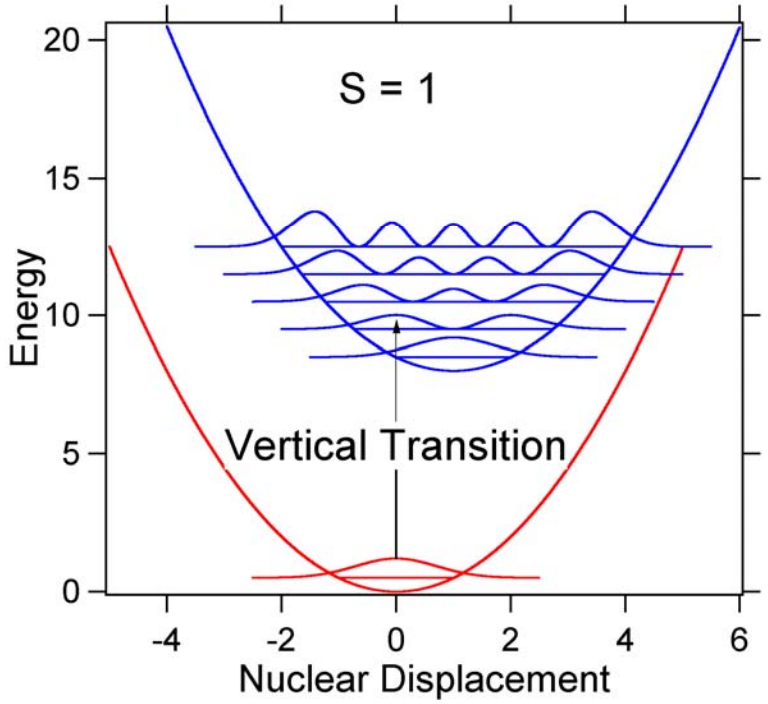

Nonemissive in solution

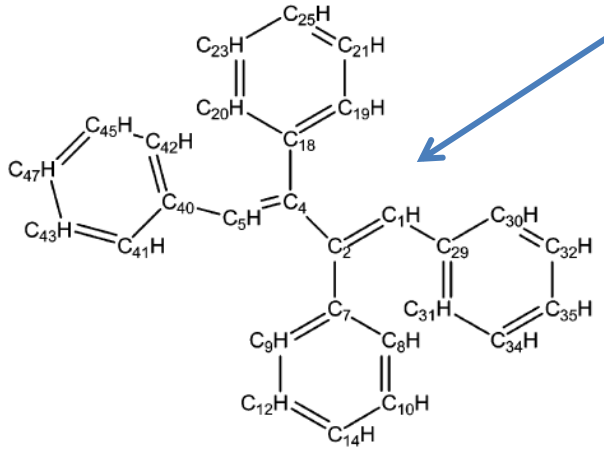

Compound 1

Strongly emissive in solution

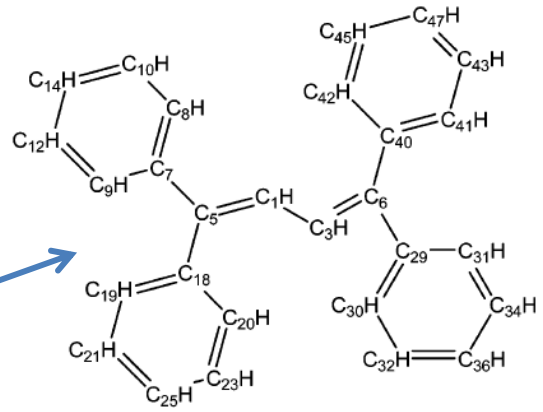

Compound 2

Figure 1. Molecular structures of the two compounds.

Qian Peng,† Yuanping Yi,† Zhigang Shuai,*,† and Jiushu Shao‡

J. AM. CHEM. SOC. 2007, *129*, 9333–9339 ■ 9333

What is common to all these phenomena?

At the most basic level, the need to compute a time dependent overlap

$$c(t) = \left\langle \Psi \left| \exp\left(-\frac{iHt}{\hbar} \right) \right| \Psi \right\rangle$$

For example, an absorption spectrum would be

$$P(\omega;\beta) = \frac{Z(\omega;\beta)}{Tr\left[e^{-\beta H_s}\right]} \qquad Z(\omega;\beta) = \frac{\hbar}{2\pi}\int_{-\infty}^{\infty} d\tau e^{-i\tau(\Delta E - \hbar\omega)}\chi(\tau,\beta)$$

$$\chi(\tau,\beta) = Tr\left[e^{-i\tau H_*}e^{-(\beta - i\tau)H_s}\right]$$

Quantum Dynamics Methods

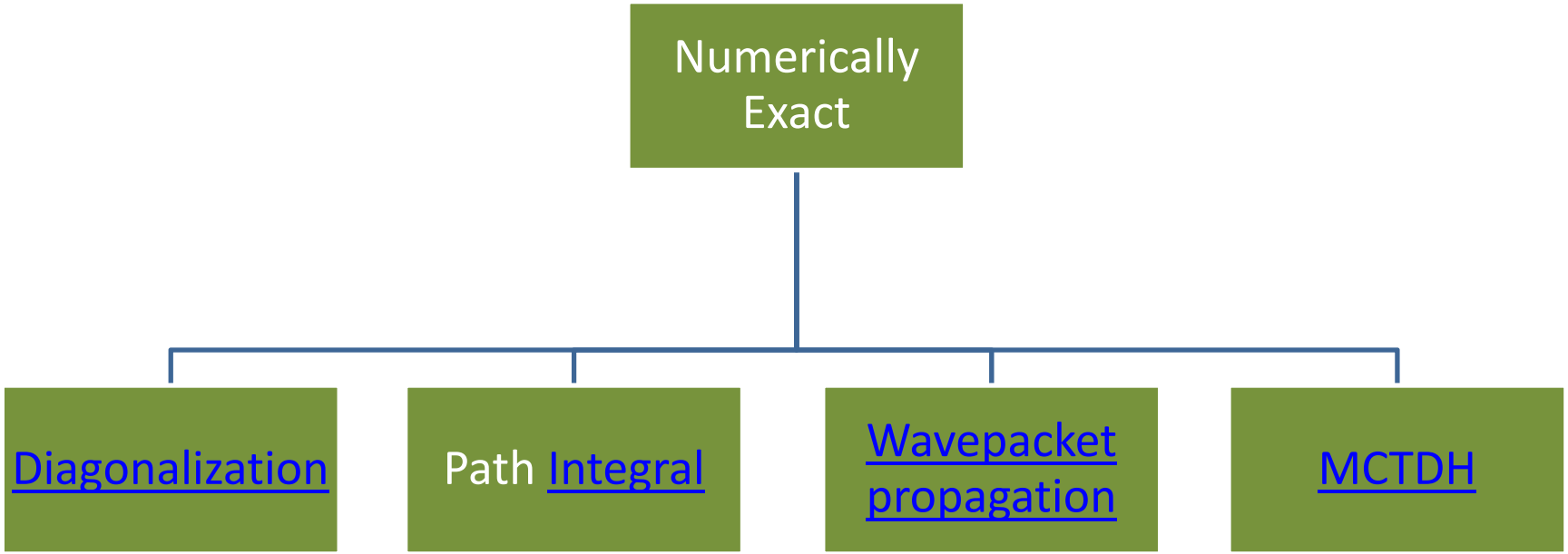

Diagonalization

$$H\,|\psi_n> = E_n\,|\psi_n>$$

Use convenient (orthonormal) basis set, create Hamiltonian matrix

$$H_{mn} = \left\langle \varphi_m \middle| H \middle| \varphi_n \right\rangle$$

and diagonalize to obtain eigenvalues and eigenvectors:

$$\det\left[\underline{H} - E\,\underline{I}\right] = 0$$

Project wavefunction onto eigenfunction basis so that:

$$c(t) = \sum_{n=0}^{\infty} \left|\langle \psi_n \,|\, \Psi \rangle\right|^2 \exp\left(-\frac{iE_n t}{\hbar}\right)$$

Deficiencies:

1. Difficult to apply to scattering (continuum problems)
2. Exponential growth of cost with number of degrees of freedom
3. Need for a global potential energy surface

Path integral methods

$$\left\langle \underline{x}\left|\exp\left(-\frac{iHt}{\hbar}\right)\right|\underline{x}'\right\rangle \sim \sum D\underline{q}(t)\exp\left(\frac{i}{\hbar}\int_0^t dt'\left[\frac{M}{2}\left(\frac{d\underline{x}}{dt'}\right)^2 - V\left(\underline{x}_{t'}\right)\right]\right)$$

Advantages:

- Amenable to Monte Carlo methods - especially useful in imaginary time computations.
- Readily parallelized
- Only local force field information needed along each path
- Useful for problems with dissipation due to influence functional

Disadvantage:

Oscillatory integrand prevents convergence, especially as time increases.

Wavepacket propagation
Split operator Fast Fourier Transform technique

R. Kosloff, J. Phys. Chem. Vol. 92, 2087 (1988).

$$\exp\left(-\frac{iH}{\hbar}t\right)=\left[\exp\left(-\frac{iH}{\hbar}\frac{t}{N}\right)\right]^{N}$$

$$\exp\left(-\frac{iH}{\hbar}\frac{t}{N}\right)\sim\exp\left(-\frac{iV(\underline{x})}{2\hbar}\frac{t}{N}\right)\exp\left(-\frac{i\underline{p}^{2}}{2M\hbar}\frac{t}{N}\right)\exp\left(-\frac{iV(\underline{x})}{2\hbar}\frac{t}{N}\right)$$

Initial wavefunction is put on a grid,
propagating the first part is a multiplication.
To carry out the momentum part one FFT's the spatial wavefunction and multiplies.
The third part is obtained by first inverse FT and again multiplication.

Advantages – Use of FFT method reduces cost to NlogN.
Ease of programming

Disadvantages - Grid based method, exponential increase of cost with dimensionality

Example – Three dimensional (vertical) scattering of an Ar atom on a LiF(100) surface.

A. Azuri and E. Pollak, to be published

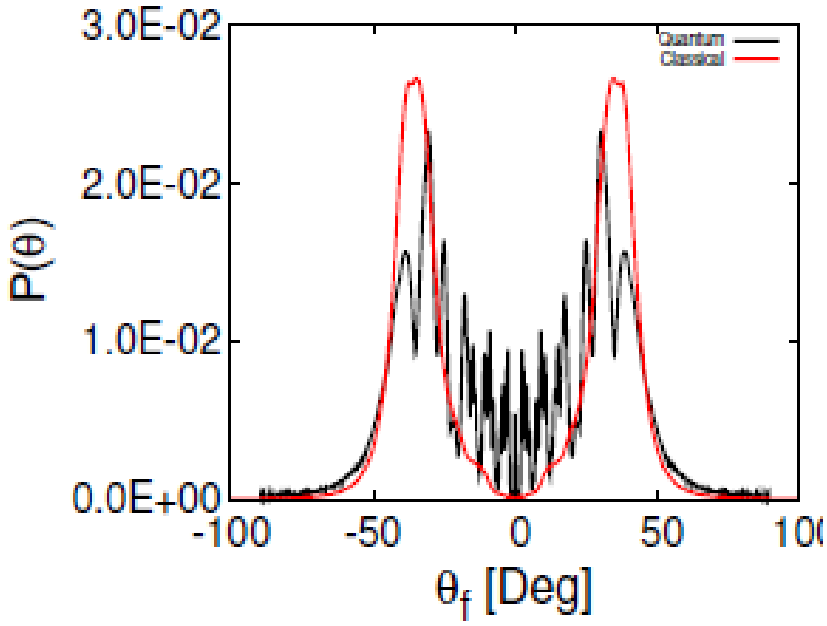

Multi-Configuration Time Dependent Hartree method

H.D. Meyer, http://www.pci.uni-heidelberg.de/cms/mctdh.html

Philosophy:

Initial wavepacket can usually be described well with a linear combination of typically 1 – 100 Hamiltonian eigenfunctions *irrespective of the dimensionality*. The ensuing time evolution occurs in this small subspace and physically, there is no exponential increase of the space with dimensionality.

The heart of the MCTDH method is creating a time evolving subspace and its optimization using the Dirac Frenkel variational principle. This limits the basis set size and allows for computation with an Increased number of degrees of freedom.

$$|\Psi(t)\rangle = \sum_J A_J(t)|\Phi_J(t)\rangle = \sum_{j_1}\sum_{j_2}\dots\sum_{j_p} A_{j_1 j_2 \dots j_p}(t)\prod_{\kappa=1}^{p}|\varphi_{j_\kappa}^{(\kappa)}(t)\rangle, \qquad p \le f.$$

Some applications of MCTDH theory

Multistate vibronic interactions in difluorobenzene radical cations. II. Quantum dynamical simulations

Shirin Faraji, H.-D. Meyer, and Horst Köppel

Citation: The Journal of Chemical Physics **129**, 074311 (2008); doi: 10.1063/1.2958918

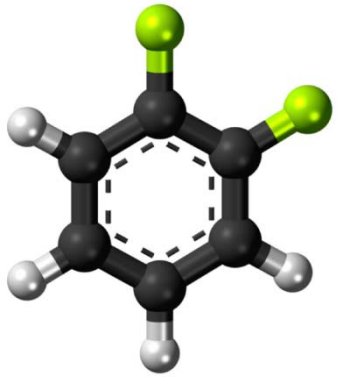

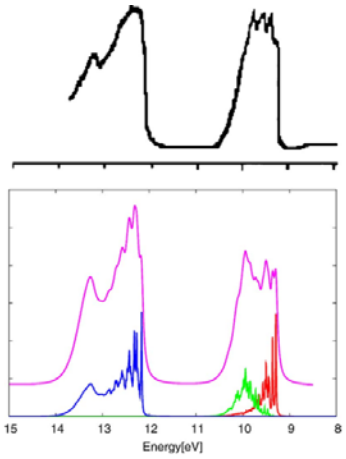

FIG. 1. (Color online) Comparison of theoretical (lower panel) and experimental (upper panel) (Ref. 39) photoelectron spectra of *o*-difluorobenzene isomer. The linewidths of the theoretical spectra are FWHM=66.6 meV (upper curve) and 13.3 meV (lower curve). In the higher-resolution theoretical spectrum, the $\tilde{X}$-$\tilde{A}$ electronic bands are drawn separately.

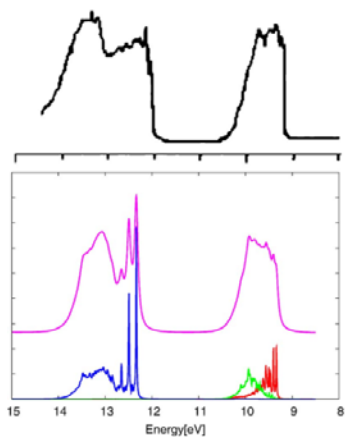

FIG. 2. (Color online) Comparison of theoretical (lower panel) and experimental (upper panel) (Ref. 39) photoelectron spectra of *m*-difluorobenzene isomer. The linewidths of the theoretical spectra are FWHM=66.6 meV (upper curve) and 13.3 meV (lower curve). In the higher-resolution theoretical spectrum, the various electronic bands are drawn separately.

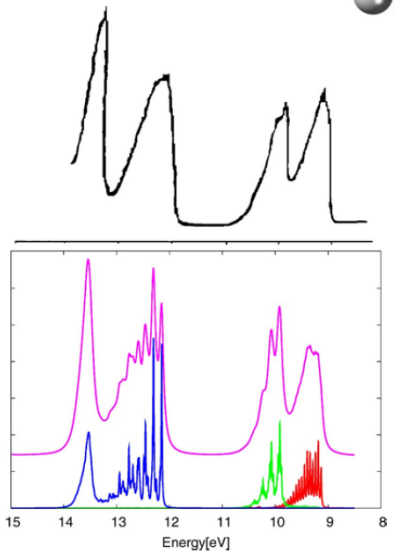

FIG. 3. (Color online) Comparison of theoretical (lower panel) and experimental (upper panel) (Ref. 39) photoelectron spectra of *p*-difluorobenzene isomer. The linewidths of the theoretical spectra are FWHM=66.6 meV (upper curve) and 13.3 meV (lower curve). In the higher-resolution theoretical spectrum, the various electronic bands are drawn separately.

Photoelectron spectra, computation with 11 degrees of freedom and six electronic states

A full-dimensional multilayer multiconfiguration time-dependent Hartree study on the ultraviolet absorption spectrum of formaldehyde oxide

Qingyong Meng and Hans-Dieter Meyer

Citation: The Journal of Chemical Physics **141**, 124309 (2014); doi: 10.1063/1.4896201

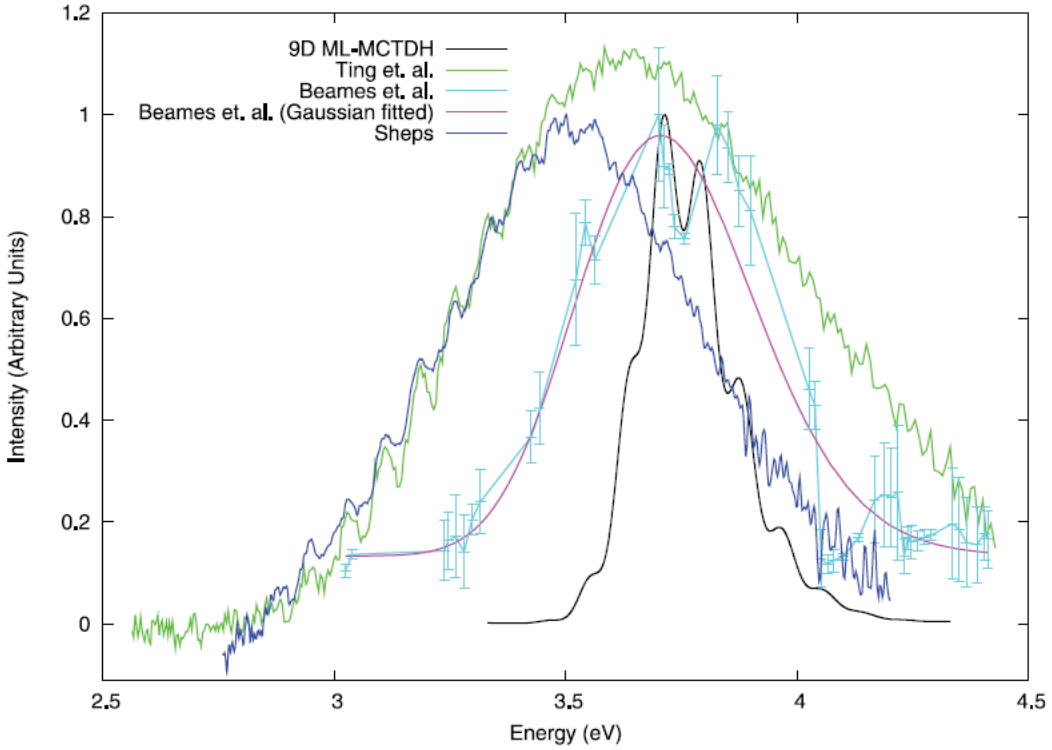

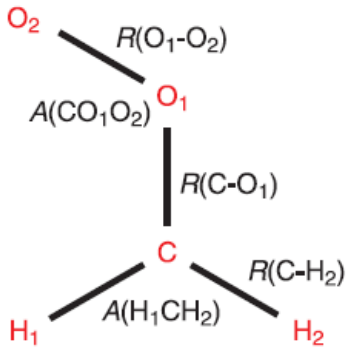

FIG. 4. Comparison of the 9D ML-MCTDH theoretical vs the experimental UV absorption spectra[5,10,16] of the $\tilde{B}\,^1A'$ band of formaldehyde oxide. The 9D ML-MCTDH theoretical spectrum is obtained via a Fourier-transform of the auto-correlation function. The spectrum is then broadened by convoluting it with a Gaussian. The resulting resolution is 55 meV FWHM. The experimental UV spectrum and its Gaussian fit drawing in the bright blue and purple lines, respectively, are reprinted with permission from Beames *et al.*, J. Am. Chem. Soc. **134**, 20045 (2012). Copyright 2012 American Chemical Society. The experimental UV spectrum drawn in the blue line is reprinted with permission from L. Sheps, J. Phys. Chem. Lett. **4**, 4201–4205 (2013). Copyright 2013 American Chemical Society. The experimental UV spectrum drawing in the green line is reprinted with permission from Ting *et al.*, Phys. Chem. Chem. Phys. **16**, 10438 (2014). Copyright 2014 The Owner Societies.

A generalised 17-state vibronic-coupling Hamiltonian model for ethylene

Joaquim Jornet-Somoza, Benjamin Lasorne, Michael A. Robb, Hans-Dieter Meyer, David Lauvergnat, and Fabien Gatti

Citation: The Journal of Chemical Physics **137**, 084304 (2012); doi: 10.1063/1.4745861

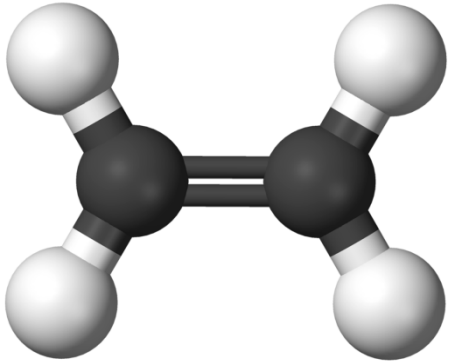

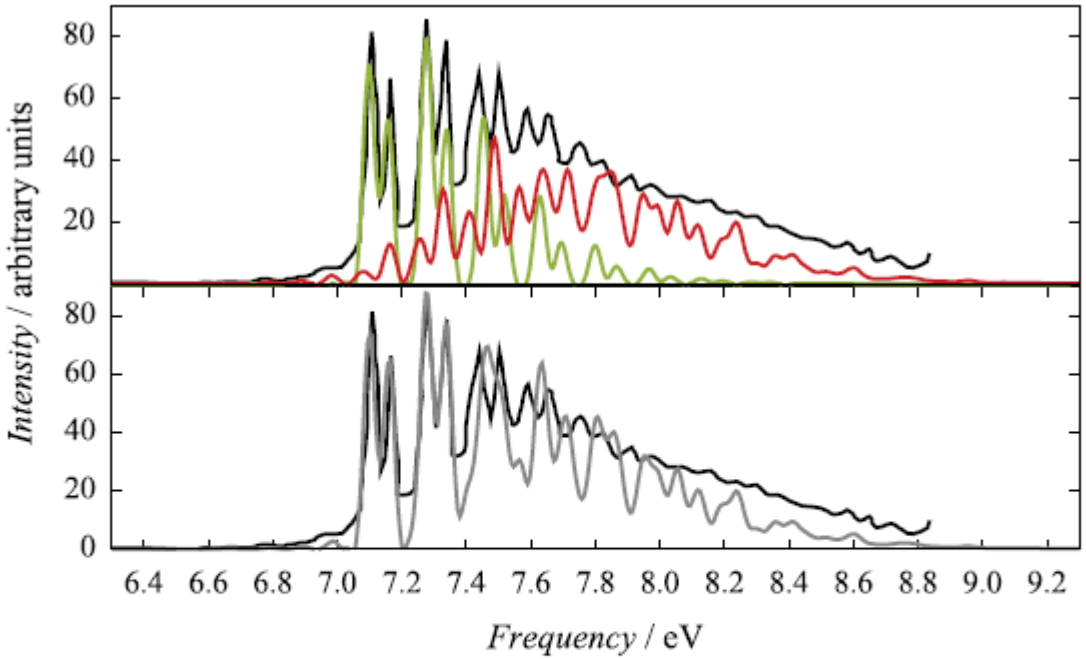

FIG. 8. Upper panel: Simulated absorption spectra for the $R(3s) \leftarrow N$ transition (green line) and the $V \leftarrow N$ transition (red line). Lower panel: Cumulative spectrum for the two transitions (grey line). The experimental absorption spectrum is shown in both cases for comparison (black line).[34] Adapted with permission from Ref. 34.

A multilayer MCTDH study on the full dimensional vibronic dynamics of naphthalene and anthracene cations

Qingyong Meng[a] and Hans-Dieter Meyer[b]

THE JOURNAL OF CHEMICAL PHYSICS **138**, 014313 (2013)

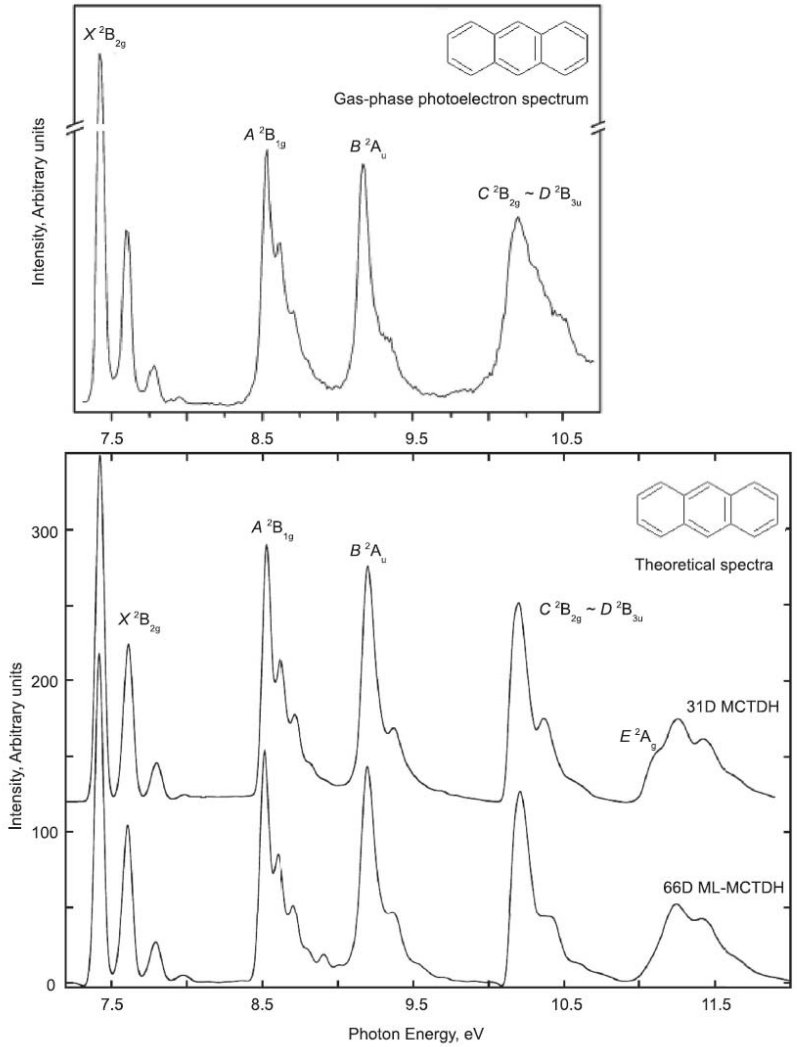

ıe as Figure 2, except for anthracene radical cation. Note that the full and reduced dimensionalities in the present simulations for anthracene radical ›D and 31D, respectively. The resolution of the computed spectra is set to 64 meV FWHM. (Upper panel) Reprinted with permission from R. S. rera, V. Coropceanu, D. A. da Silva Filho, R. Friedlein, W. Osikowicz, R. Murdey, C. Suess, W. R. Salaneck, and J.-L. Bredas, J. Phys. Chem. B 2006). Copyright 2006 American Chemical Society.

Semiclassics

Semiclassical Initial Value Representations

M.F. Herman and E. Kluk, Chem. Phys. **91**, 27 (1984).

K. G. Kay, J. Chem. Phys. **100**, 4377,4432; **101**, 2250 (1994).

General structure of semiclassical IVR propagator:

$$\hat{K}_{IVR}(t) = \int_{-\infty}^{\infty} \frac{d\underline{p}d\underline{q}}{(2\pi\hbar)^N} D(\underline{p},\underline{q},t) e^{\frac{i}{\hbar}W(\underline{p},\underline{q},t)} \mid g(\underline{p},\underline{q},t) >< g(\underline{p},\underline{q},0) \mid$$

The coherent state is a Gaussian wavepacket with a time evolving center – q(t); time evolving momentum – p(t); and time evolving width – Γ(t):

$$< \underline{x} \mid g(\underline{p},\underline{q},t) >= \left(\frac{\det[\underline{\Gamma}(t)]}{\pi^N} \right)^{\frac{1}{4}} e^{-\frac{1}{2}[\underline{x}-\underline{q}(t)]^T \underline{\Gamma}(t)[\underline{x}-\underline{q}(t)]+\frac{i}{\hbar}\underline{p}(t)[\underline{x}-\underline{q}(t)]}$$

D(p,q,t) is a prefactor dependent on monodromy matrix elements.

Completeness:

$$\int_{-\infty}^{\infty} \frac{d\underline{p}\,d\underline{q}}{(2\pi\hbar)^N} \left| g(\underline{p},\underline{q};t) \right\rangle \left\langle g(\underline{p},\underline{q};t) \right| = I$$

A "good" IVR propagator is exact for harmonic systems (just as is the zero-th order solution of the Wigner-Liouville equation) and is unitary in the stationary phase sense.

Appeal of SCIVR – can be carried out on the fly using Monte Carlo methods.

Some recent applications

The absorption spectrum of Formaldehyde (6 degrees of freedom)

J. Tatchen and E. Pollak, J. Chem. Phys. **130**, 041103 (2009).

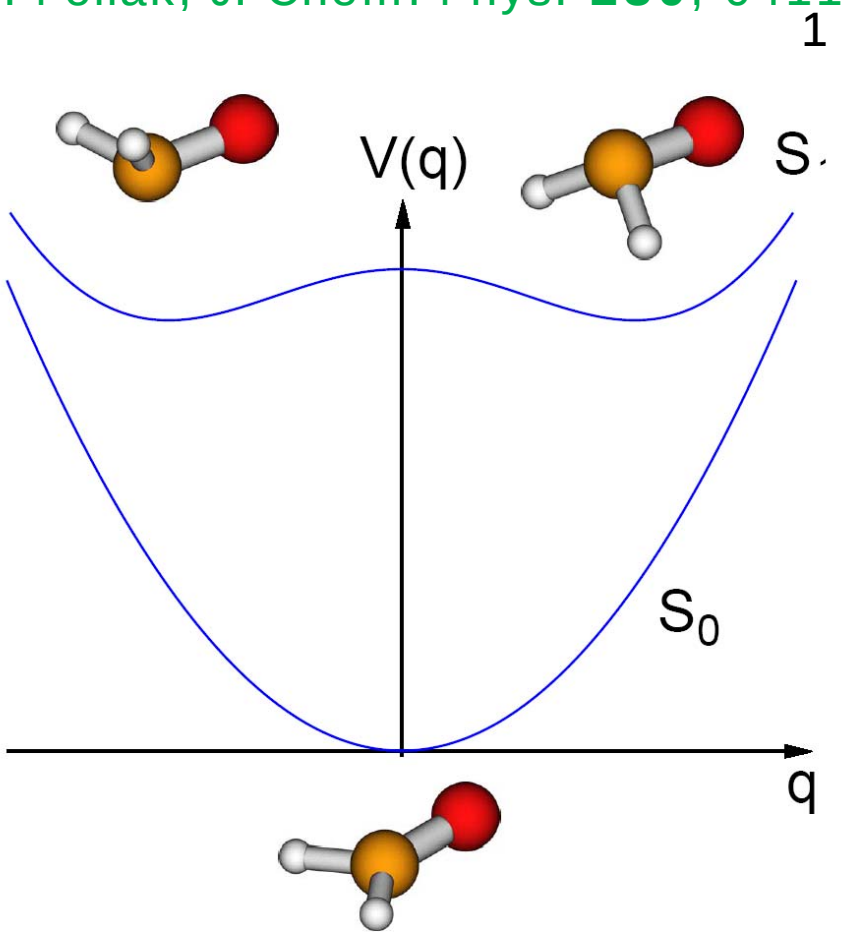

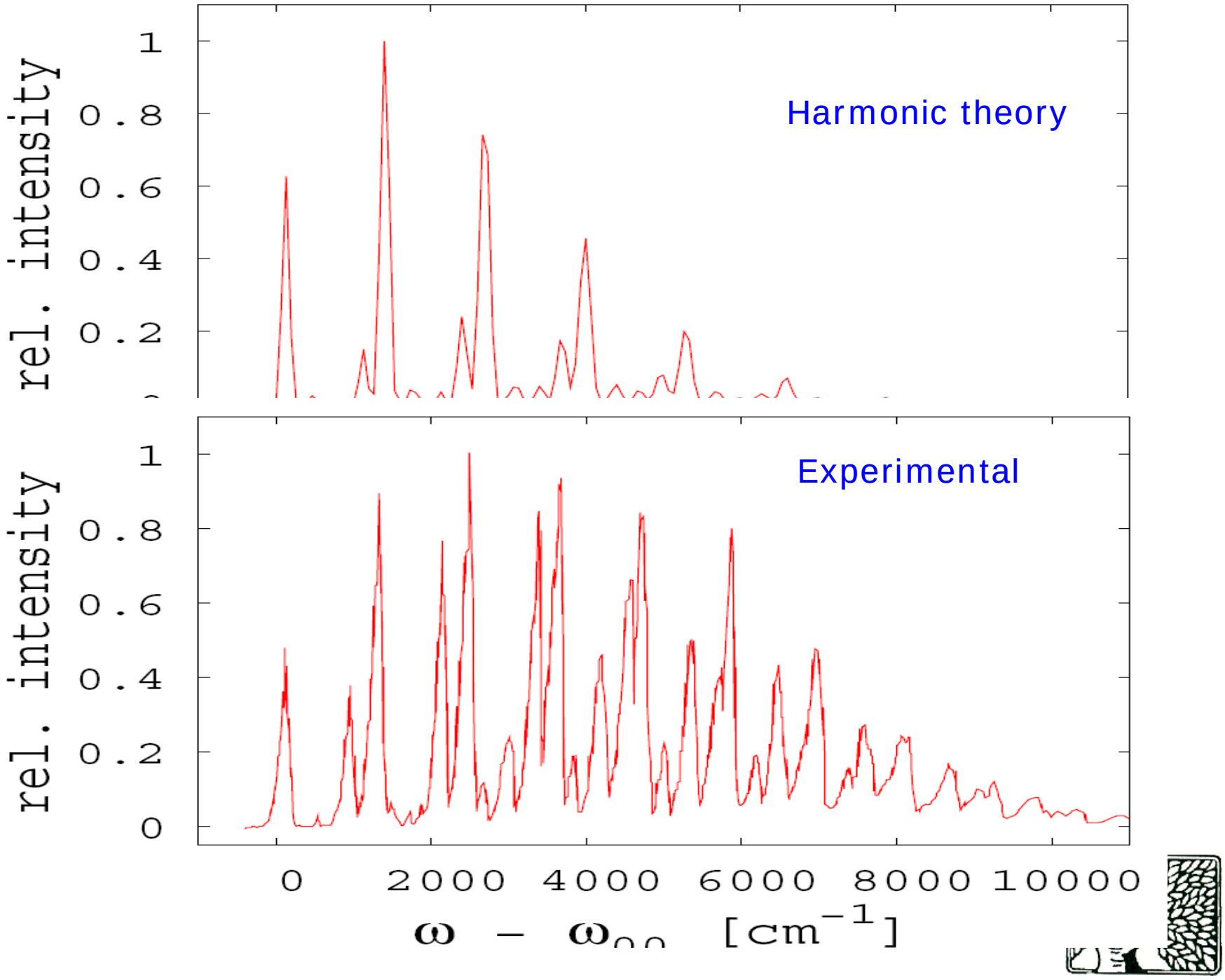
Harmonic theory
Experimental
rel. intensity
rel. intensity
0
0.2
0.4
0.6
0.8
1
0
2000
4000
6000
8000
10000
ω − ω00 [cm−1]

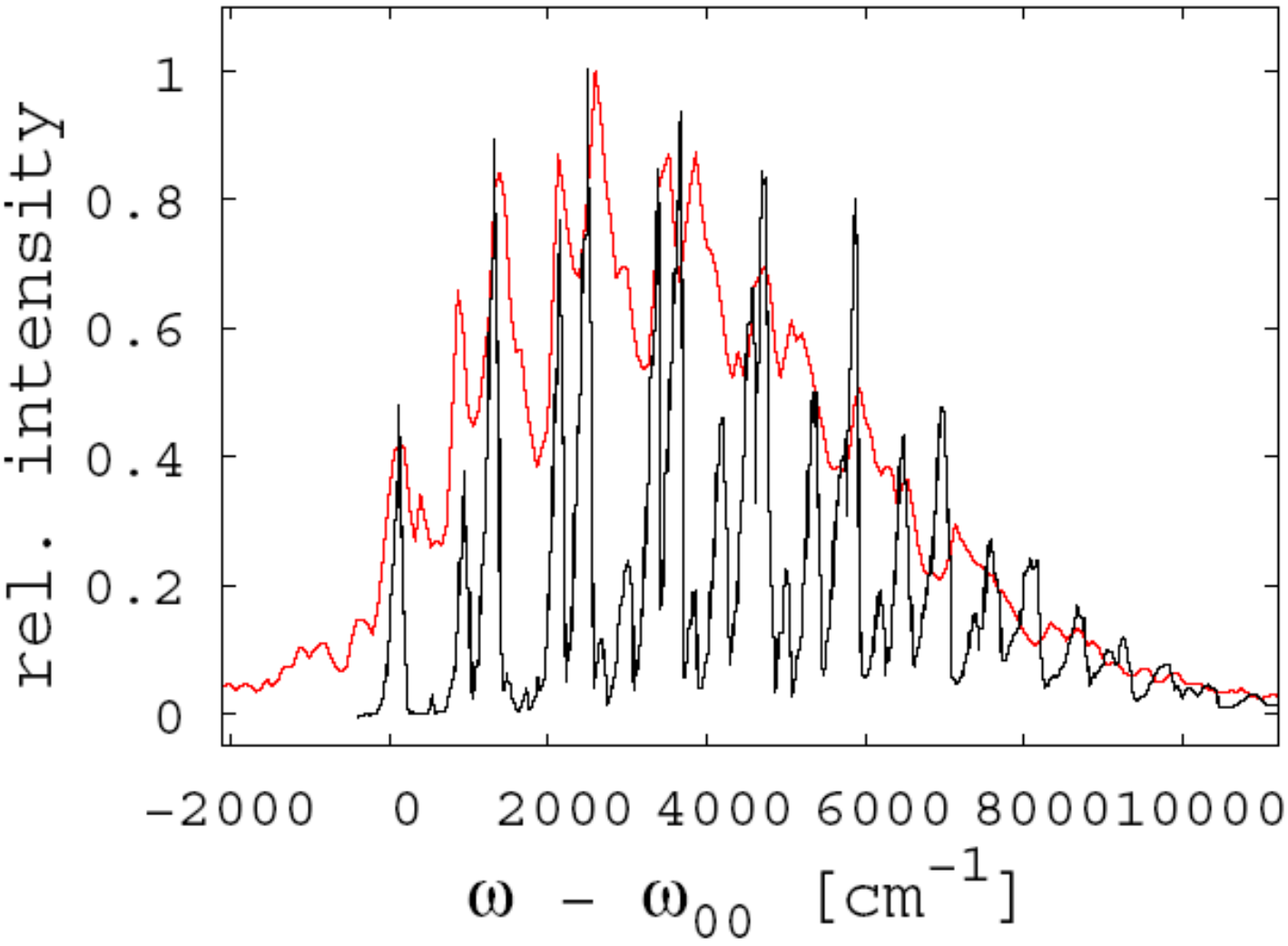

SCIVR details – 5680 trajectories integrated for 500 fsec,
TDDFT for excited state using B3LYP like
functional (turbomole program)

Reproducing Deep Tunneling Splittings, Resonances, and Quantum Frequencies in Vibrational Spectra From a Handful of Direct Ab Initio Semiclassical Trajectories

Riccardo Conte,[†] Alán Aspuru-Guzik,[‡] and Michele Ceotto*[,§]

J. Phys. Chem. Lett. **4**, 3407 (2013)

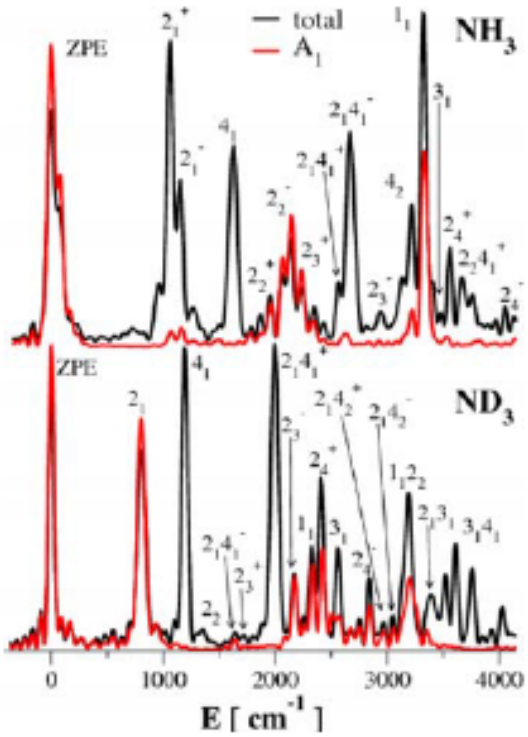

Figure 3. Ab initio direct simulations of the vibrational spectra (black lines) of NH_3 (upper panel) and ND_3 (lower panel). Peaks are better assigned by comparison with the A_1 symmetry simulations (red lines). Eight trajectories have been propagated "on-the-fly". ZPEs are respectively 7342 cm^{-1} and 5370 cm^{-1}. Both vibrational peak spacings and tunneling splittings are significantly reduced after deuteration.

Table 1. Ammonia Vibrational Eigenvalues[a]

	harm.[b]	KM[c]	MC[d]	QM[e]
ZPE[f]	7575.9[g]	7464	7442	7460.9
$A_1 2_1(+)$	1108.9[h]	1003	1014	1018.3
$A_1 2_1(-)$	1108.9		1100	1030.3
E $4_1(+)$	1687.9	1619	1630	1639.5
E $4_1(-)$	1687.9		1630	1639.8
A_1 $2_2(+)$	2217.8	2073	1950	1805.3
A_1 $2_2(-)$	2217.8		2030	1975.5
A_1 $2_3(+)$	3326.7		2352	2500.5
E $2_1 4_1(+)$	2796.8	2612	2648	2645.7
E $2_1 4_1(-)$	2796.8		2724	2661.8
A_1 $2_3(-)$	3326.7		2914	2957.8
A_1 $4_2(+)$	3375.8		3252	3244.7
A_1 $4_2(-)$	3375.8		3252	3246.2
E $4_2(+)$	3375.8	3239		3268.6
E $4_2(-)$	3375.8			3269.1
A_1 $1_1(+)$	3472.6	3389	3380	3369.8
A_1 $1_1(-)$	3472.6		3380	3370.4
E $2_2 4_1(+)$	3905.7		3426	3407.0
E$3_1(+)$	3597.3	3449	3490	3474.9
E$3_1(-)$	3597.3		3490	3474.9
$A_1 2_4(+)$	4435.6		3552	3504.0
E $2_2 4_1(-)$	3905.7	3597	3676	3604.9
$A_1 2_4(-)$	4435.6		4074	4078.6
MAE	300.8	53	38	-
RMSD	331.6	97	57	-

[a]Comparison of the MC-TA-SC-IVR results (MC) with harmonic approximation ones (harm) and previous semiclassical results (KM) obtained for ammonia on the MLT PES. Exact quantum mechanical data (QM) are used as benchmark. The mean absolute error (MAE) and root-mean-square deviation (RMSD) are reported in the last two rows. [b]The harmonic level spacing. [c]Kaledin and Miller results.[2] [d]Present method with 8 trajectories and 16 reference coherent states. [e]Quantum mechanical results.[27] [f]The vibrational terms. [g]ZPE energy from the bottom of the well. [h]Energy of the vibrational levels from the ZPE value.

Determination of molecular vibrational state energies using the ab initio semiclassical initial value representation: Application to formaldehyde

Stephanie Y. Y. Wong, David M. Benoit, Marius Lewerenz, Alex Brown, and Pierre-Nicholas Roy

Citation: The Journal of Chemical Physics **134**, 094110 (2011): doi: 10.1063/1.3553179

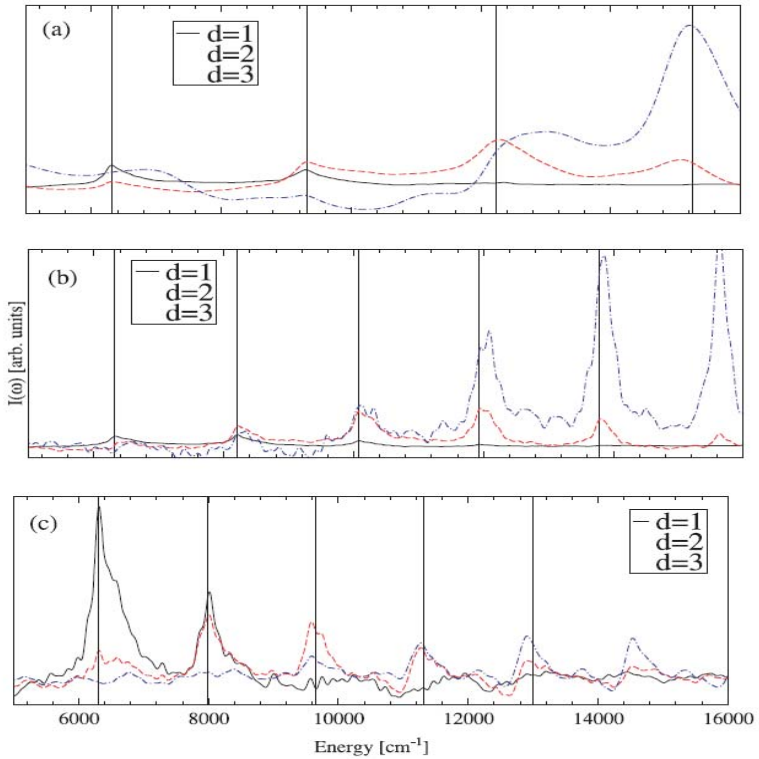

FIG. 2. Intensity (spectral density) plots from SC-IVR given symmetry-adapted reference state overlaps with displacements along the three A1 normal modes, (a) ν_1, (b) ν_2, and (c) ν_3, respectively. The curves are the SC-IVR results. d represents the magnitude of displacement (energy $\propto d^2$) of each mode (see text for details). The vertical lines represent the curvilinear-VSCF/VCIPSI-PT2 reference bound state calculation. In each panel, the left-most vertical line represents the ground vibrational state (000000), and in the case of the first panel, the subsequent lines are the (100000), (200000), (300000), and (400000) vibrational states. The other two panels are similarly labeled.

State	linear-VSCF/VCIPSI-PT2	SC-IVR
(000000)	6309	6311
(100000)	9320	9303
(010000)	8198	8208
(001000)	7980	8013
(200000)	12232	12 297
(020000)	10074	10 089
(002000)	9650	9587
(300000)	15254	15 209
(030000)	11936	11 961
(003000)	11321	11 269
(400000)	17996	17 848
(040000)	13787	13 853
(004000)	12986	12 904
MAE	—	48
RMSD	—	61

Application to internal conversion of Formaldehyde

Experimental data:

CHEMICAL PHYSICS LETTERS Volume 33, number 1 15 May 1975

SINGLE VIBRONIC LEVEL PHOTOCHEMISTRY OF FORMALDEHYDE (H_2CO, $^1A_2$): RADIATIVE AND NON-RADIATIVE TRANSITIONS*

Richard G. MILLER and Edward K.C. LEE

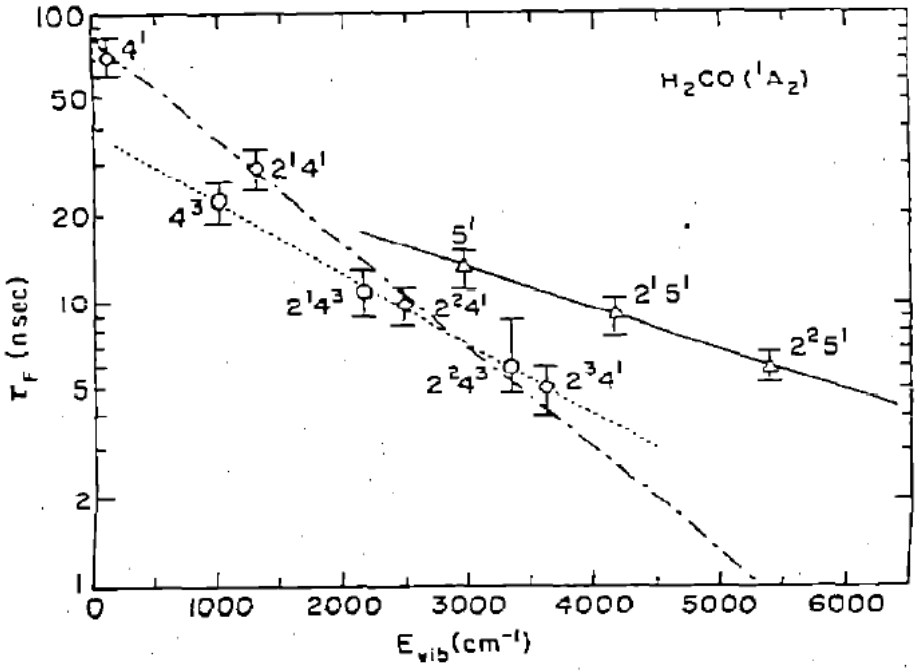

Fig. 2. Observed fluorescence decay times versus vibrational energy of H_2CO ($^1A_2$): ν'_2 = C–O stretch; ν'_4 = out-of-plane bending; ν'_5 = asymmetric C–H stretch.

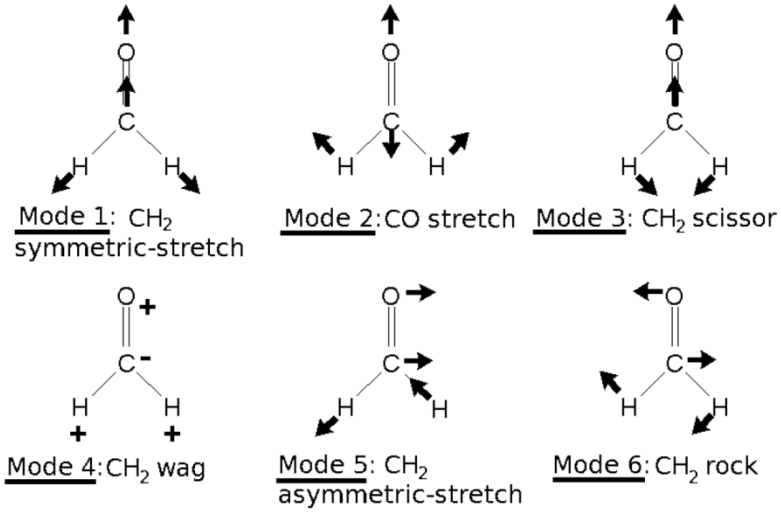

On-the-fly semiclassical study of internal conversion rates of formaldehyde

Reuven Ianconescu, Jörg Tatchen, and Eli Pollak

Citation: The Journal of Chemical Physics **139**, 154311 (2013); doi: 10.1063/1.4825040

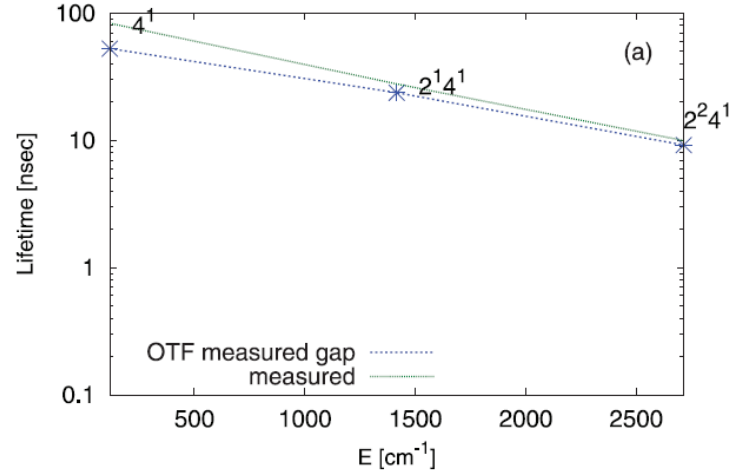

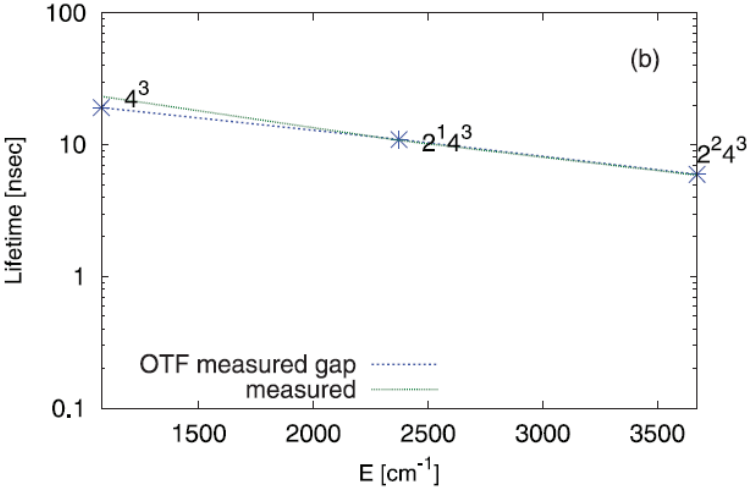

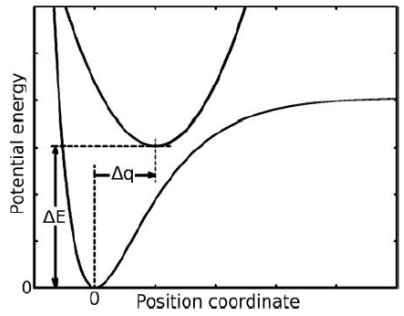

FIG. 1. Adiabatic surfaces describing the ground and excited electronic states in one dimension. Δq is the spatial shift between the surfaces, it is defined as positive if the shift is toward the dissociative side of the ground state and negative if it is toward the repulsive side. ΔE is the energy gap between the bottom of the ground and excited electronic states.

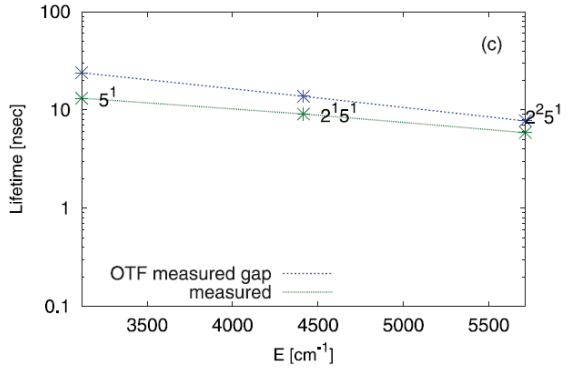

FIG. 8. Lifetimes' comparisons between measured results and the *ab initio* on the fly computation obtained after dividing the NACME slopes by 1.65. The group of states 4^1, 4^3, and 5^1 are shown in panels (a), (b), and (c), respectively.

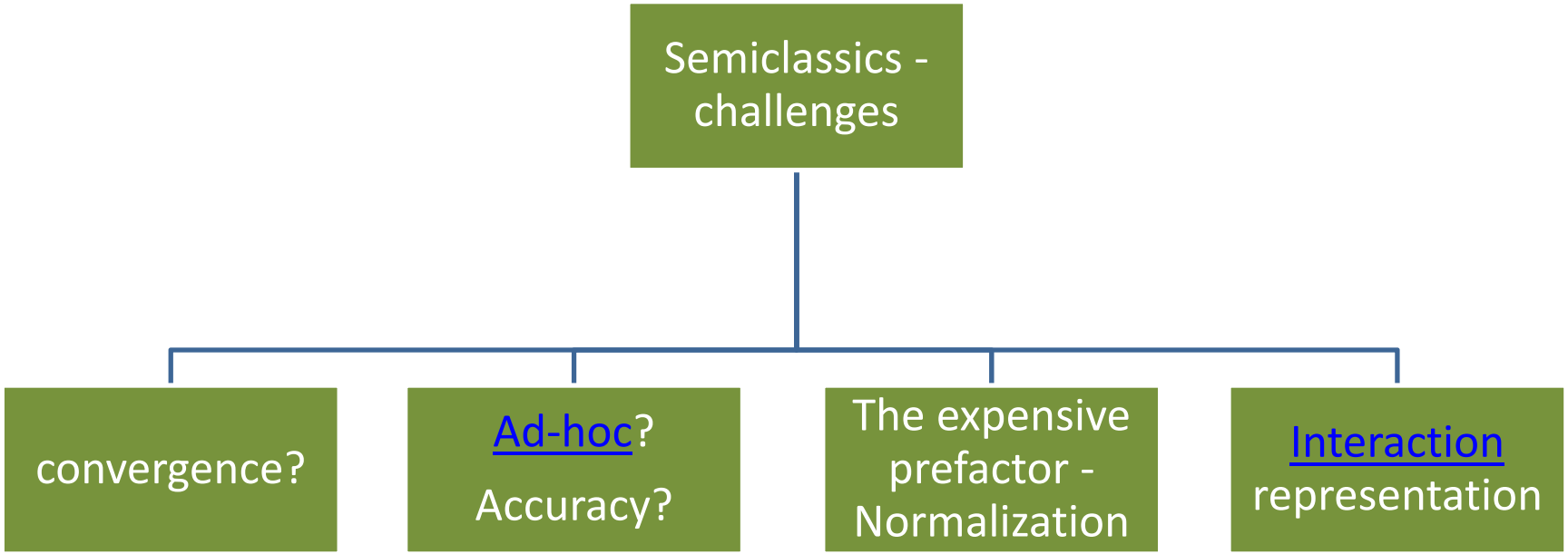
Semiclassics - challenges
convergence?
Ad-hoc?
Accuracy?
The expensive prefactor - Normalization
Interaction representation

Difficulty– MC integration of an oscillatory integrand

Consider a simple example

$$I(\alpha) = \int_{-\infty}^{\infty} dx e^{-x^2} \cos(\alpha x)$$

$$= \int_{-\infty}^{\infty} dx e^{-x^2} \cos(\alpha x)[\theta(\cos(\alpha x)) + \theta(-\cos(\alpha x))]$$

$$\equiv I_+(\alpha) - |I_-(\alpha)|$$

Let the results of the MC integration be:

$$I_+(\alpha) = \langle I_+(\alpha) \rangle + \Delta I_+(\alpha), \qquad I_-(\alpha) = \langle I_-(\alpha) \rangle + \Delta I_-(\alpha)$$

Even if the relative error in I_+ and I_- is small, the relative error for the full integral may be very large especially if $I_+ \sim I_-$ which is the case when $\alpha >> 1$:

$$I(\alpha) = \langle I_+(\alpha) \rangle - |\langle I_-(\alpha) \rangle| + \Delta I_+(\alpha) + \Delta I_-(\alpha)$$

Ad-hoc? Thawed Gaussian? Frozen Gaussian?

Generalized time dependent perturbation theory:

J. Ankerhold, M. Saltzer and E. Pollak, J. Chem. Phys. 116, 5925 (2002).

E. Pollak and J. Shao, J. Phys. Chem. A **107**, 7112 (2003).

S. Zhang and E. Pollak, Phys. Rev. Lett. **91**, 190201 (2003); J. Chem. Phys. **119**, 11058 (2003).

$$\hat{K}_{IVR}(t) = \int_{-\infty}^{\infty} \frac{d\,\underline{p}d\,\underline{q}}{(2\pi\hbar)^N} D(\underline{p},\underline{q},t) e^{\frac{i}{\hbar}W(\underline{p},\underline{q},t)} \,|\, g(\underline{p},\underline{q},t) >< g(\underline{p},\underline{q},0) \,|$$

$$i\hbar \frac{\partial K_{IVR}(t-t')}{\partial t} = \hat{H}\hat{K}_{IVR}(t-t') + \hat{C}(t-t'); \qquad \hat{K}_{IVR}(0) = \hat{I}$$

The general structure of the "correction operator":

$$\hat{C}(t) = \int_{-\infty}^{\infty} \frac{dpdq}{2\pi\hbar} \Delta V(\hat{x},p,q,t) D(p,q,t) e^{\frac{i}{\hbar}W(p,q,t)} \,|\, g(p,q,t) >< g(p,q,0) \,|$$

Typically, ΔV depends only on the nonharmonic part of the potential.

$$i\hbar \frac{\partial \hat{K}_{IVR}(t-t')}{\partial t} = \hat{H}\hat{K}_{IVR}(t-t') + \hat{C}(t-t'); \qquad \hat{K}_{IVR}(0) = \hat{I}$$

$$i\hbar \frac{\partial \hat{K}(t-t')}{\partial t} = \hat{H}\hat{K}(t-t') \qquad \hat{K}(0) = \hat{I}$$

=> $$\hat{K}_{IVR}(t-t') = \hat{K}(t-t') + \frac{1}{i\hbar}\int_{t'}^{t} ds \hat{K}(t-s)\hat{C}(s)$$

SCIVR series expansion: $$\hat{K} = \sum_{j=0}^{\infty} \hat{K}_j, \qquad \hat{K}_j \sim \hat{C}^j$$

$$\hat{K}_1(t-t') = \frac{i}{\hbar}\int_{t'}^{t} ds \hat{K}_0(t-s)\hat{C}(s); \qquad \hat{K}_j(t-t') = \frac{i}{\hbar}\int_{t'}^{t} ds \hat{K}_{j-1}(t-s)\hat{C}(s)$$

Coherent classical path description of tunneling

D.-H. Zhang and E. Pollak, Phys. Rev. Lett. **93**, 140401 (2004).

Transmission of an incident Gaussian wavepacket through a symmetric Eckart Barrier, with average energy = half of barrier height:

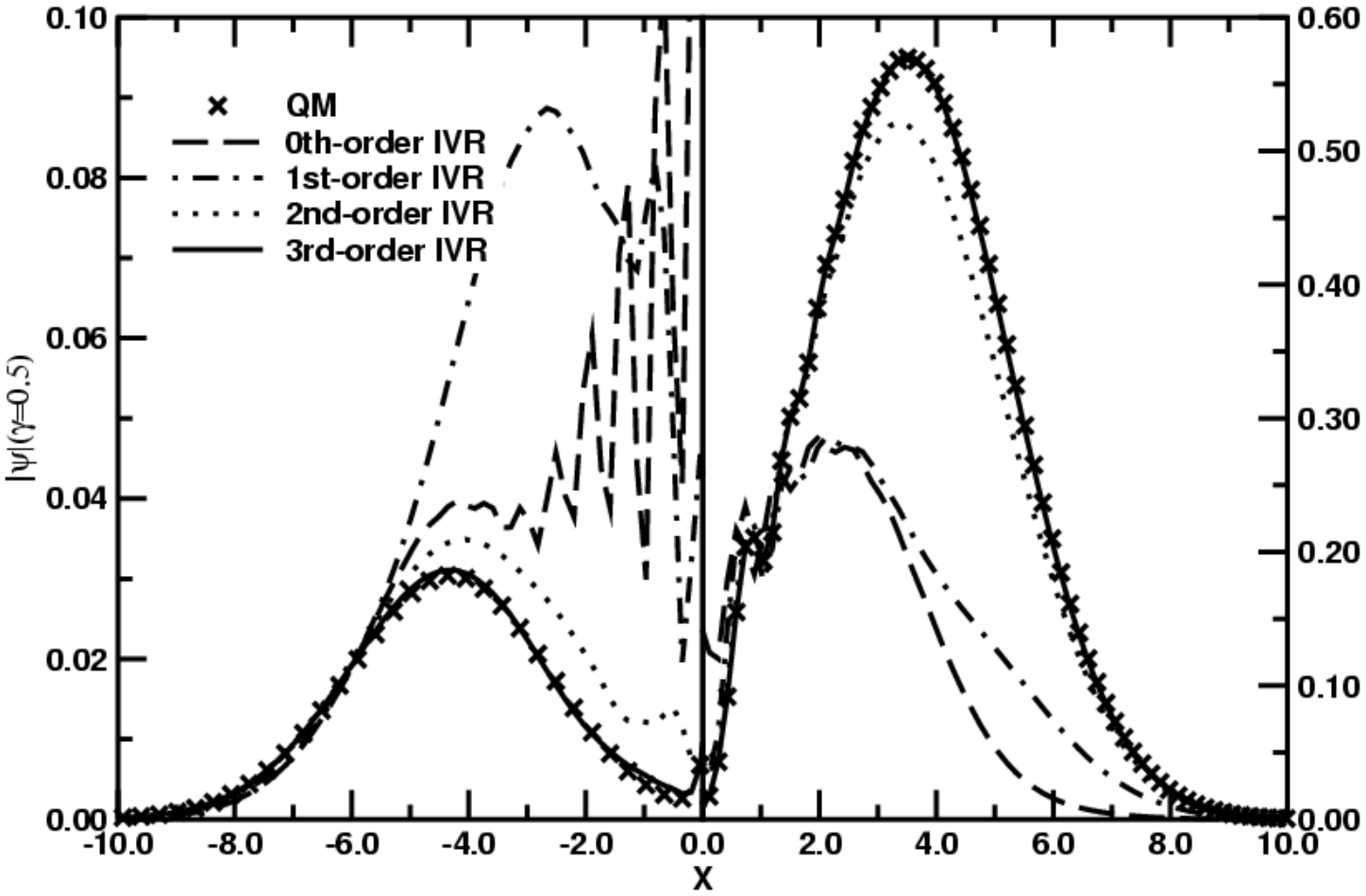

Coherent classical paths

Zero-th order:

An above barrier trajectory evolves the wavepacket from one side of the barrier to the other

1-st order:

A trajectory evolves to time τ then there is a "jump" in phase space, then the packet is evolved to time t:

$$\left|\psi(t)\right\rangle = \left[\hat{K}_0(t) + \hat{K}_1(t) + \ldots\right]\psi(0)\rangle = \left[\hat{K}_0(t) + \int_0^t d\tau \hat{K}_0(t-\tau)\hat{C}(\tau) + \ldots\right]\left|\psi(0)\right\rangle$$

$$\hat{K}_0(t)\left|\psi(0)\right\rangle = \int_{-\infty}^{\infty} \frac{dpdq}{2\pi\hbar} R(\tau) e^{\frac{i}{\hbar}W(t)} \left|g(p,q;\tau)\right\rangle\left\langle g(p,q;0)\middle|\psi(0)\right\rangle$$

$$\hat{K}_1(t)\left|\psi(0)\right\rangle = \int_0^t d\tau \int_{-\infty}^{\infty} \frac{dp'dq'}{2\pi\hbar} \int_{-\infty}^{\infty} \frac{dpdq}{2\pi\hbar} R(\tau)R'(t-\tau) e^{\frac{i}{\hbar}[W'(t-\tau)+W(\tau)]}$$
$$\cdot\left|g(p',q';t-\tau)\right\rangle\left\langle g(p',q';0\middle|\Delta V\middle|g(p,q;\tau)\right\rangle\left\langle g(p,q;0)\middle|\psi(0)\right\rangle$$

b. Quantum diffraction

R. Gelabert, X. Gimenez, M. Thoss, H. Wang and W.H. Miller, J. Chem. Phys. **114**, 2572 (2001).

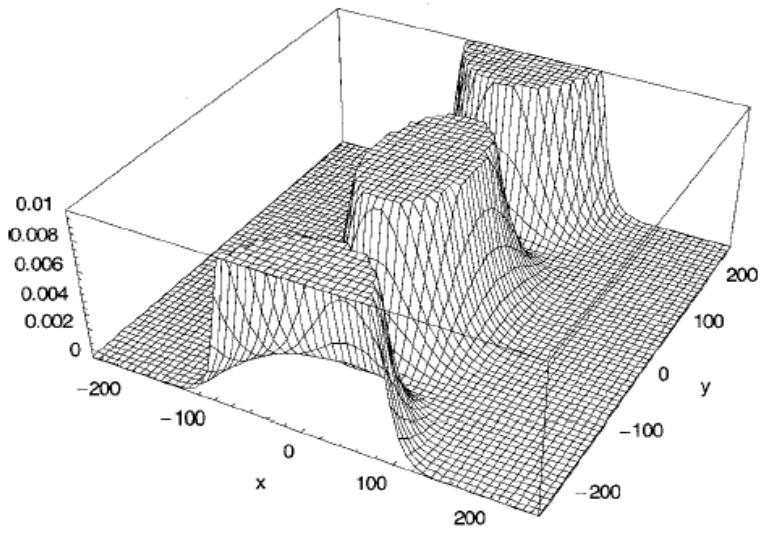

FIG. 1. Three-dimensional plot of the double slit potential energy surface, Eq. (2.1). The parameters of the potential are given in the text.

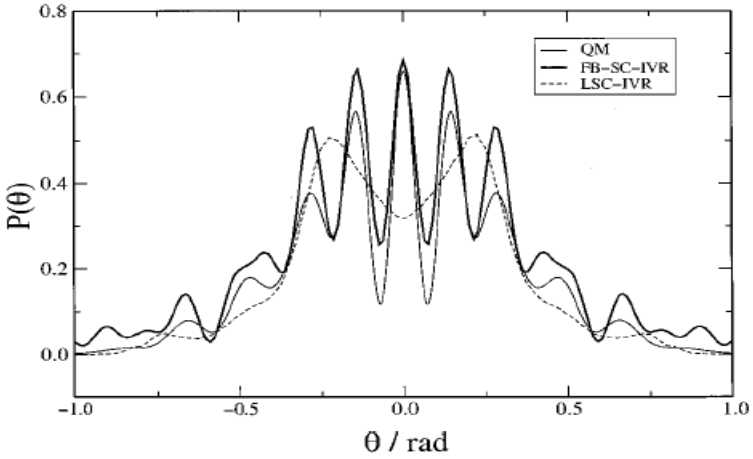

FIG. 2. Comparison of the diffraction pattern calculated according to quantum-mechanical (QM), forward–backward semiclassical initial value representation (FB-SC-IVR), and linearized semiclassical initial value representation (LSC-IVR) methods.

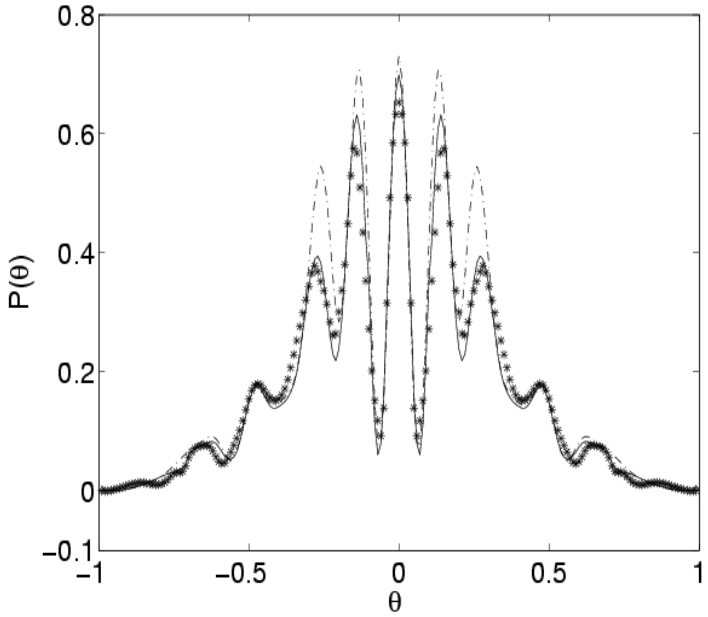

Prefactor free semiclassical IVR:

S. Zhang and E. Pollak, J. Chem. Phys. **121**, 3384 (2004).
J. Tatchen, E. Pollak, G.-H. Tao and W.H. Miller, JCP **134**, 134104 (2011).

$$\hat{K}_0(t) = \int_{-\infty}^{\infty} \frac{d\,\underline{p} d\,\underline{q}}{(2\pi\hbar)^N} e^{\frac{i}{\hbar} W(\underline{p},\underline{q},t)} \,|\, g(\underline{p},\underline{q},t) >< g(\underline{p},\underline{q},0) \,|$$

$$K_{0,N}(t) = \frac{1}{\sqrt{N_\Psi(t)}} K_0(t) \qquad N_\Psi(t) = \left\langle \Psi \middle| K_0^\dagger(t) K_0(t) \middle| \Psi \right\rangle$$

$$\begin{aligned} N_0(t) &= \langle \psi \left| K_{FG}^\dagger(t)\, K_{FG}(t) \right| \psi \rangle \\ &= \int_{-\infty}^{\infty} \frac{dpdq}{2\pi\hbar} \int_{-\infty}^{\infty} \frac{dp'dq'}{2\pi\hbar} \langle \psi | g_\Gamma(p',q') \rangle \langle g_\Gamma(p_t',q_t') | g_\Gamma(p_t,q_t) \rangle \langle g_\Gamma\,(p,q)\,|\psi\rangle \\ &\quad \exp\left(\frac{i}{\hbar} \left[S(p,q;t) - S\,(p',q';t) \right] \right). \end{aligned}$$

Difficulty: The normalization integral is still very expensive, it demands a double phase space integration. Can be reduced to a single phase space integration using a linearization approximation. Result, without phases, converges as rapidly as a classical computation.

Modeling for a Morse potential approximation to the I_2 molecule with initial Gaussian wavefunction centered about the 26th eigenvalue (~1/3 of dissociation energy):

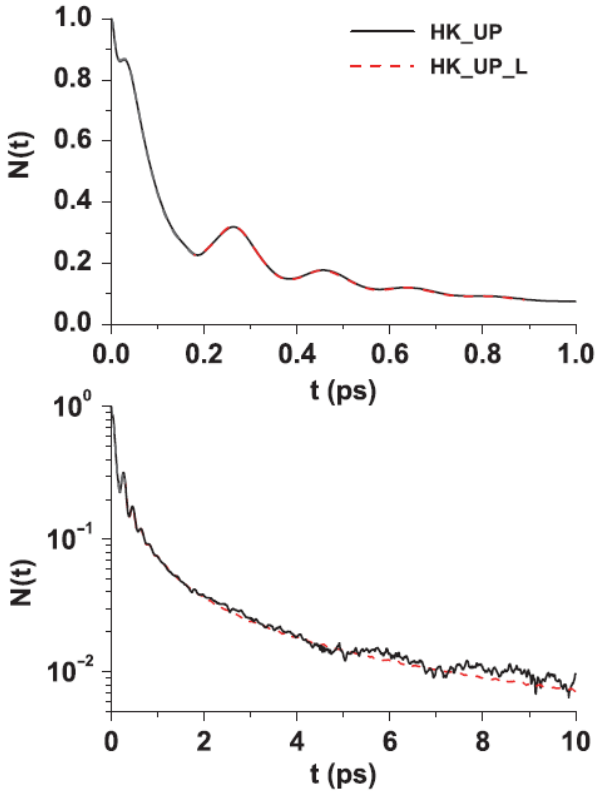

FIG. 1. Comparison of the normalization integral for the unit prefactor HK propagator without (solid line) and with (dashed line) linearization. The top panel shows the normalization integral on a linear scale and for short times. Note the rapid loss of unitarity. The bottom panel shows the long time loss of normalization on a log scale.

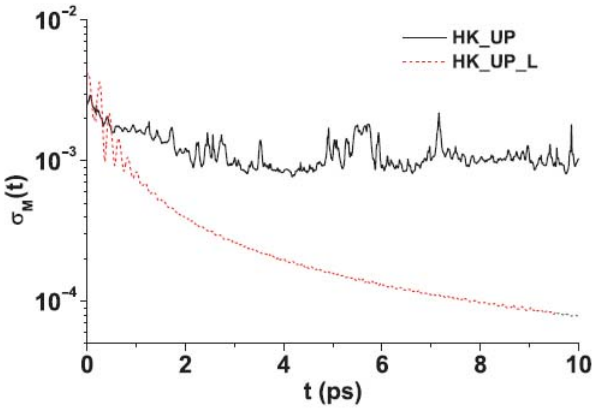

FIG. 2. The standard deviation for the normalization integral. The sample size for the exact normalization is 400 000, while the sample size used for the linearized form is 4000. Using the linearization increases the speed of computation by a factor of 1000.

Application to Formaldehyde absorption spectrum:

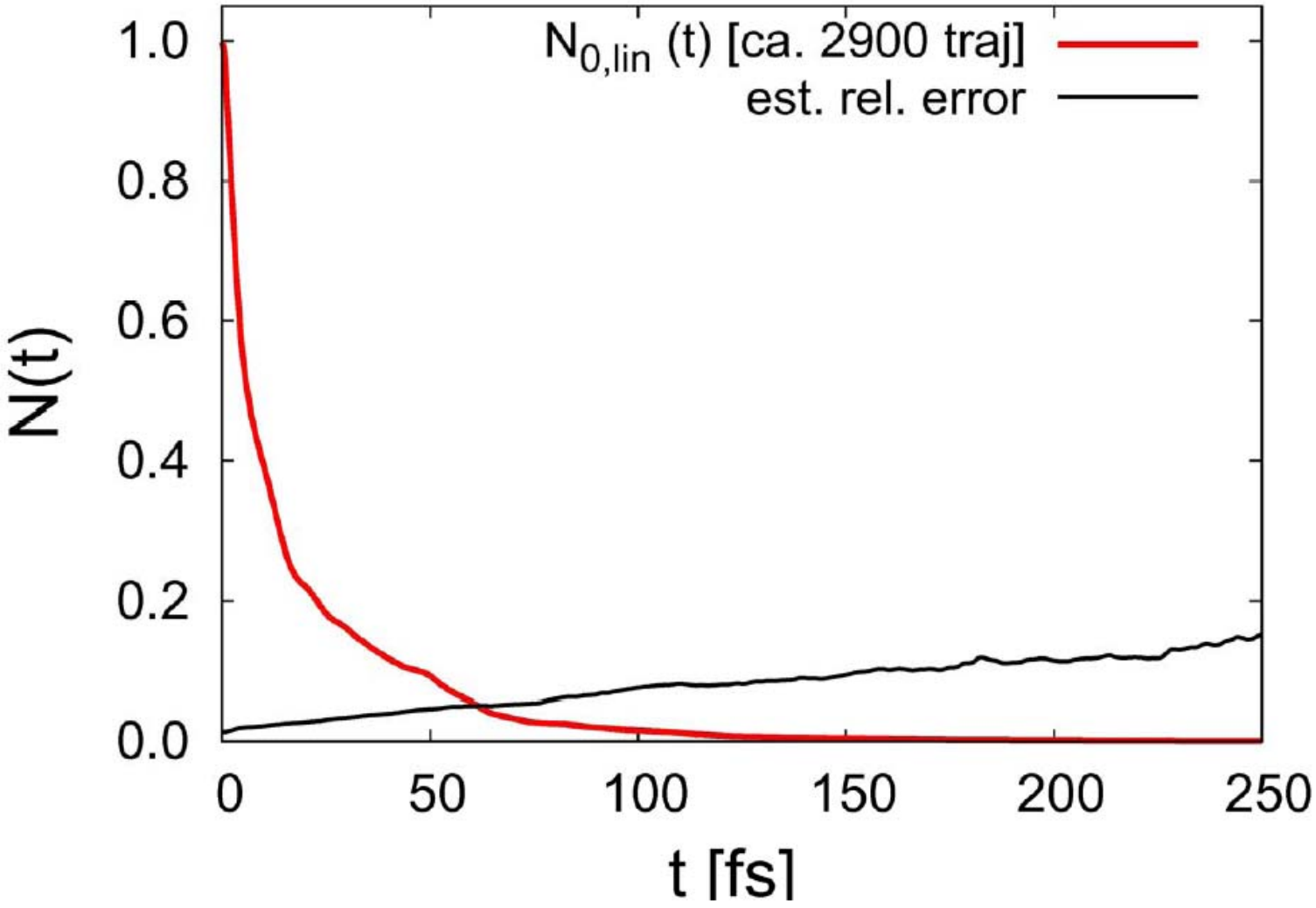

The renormalized absorption spectrum

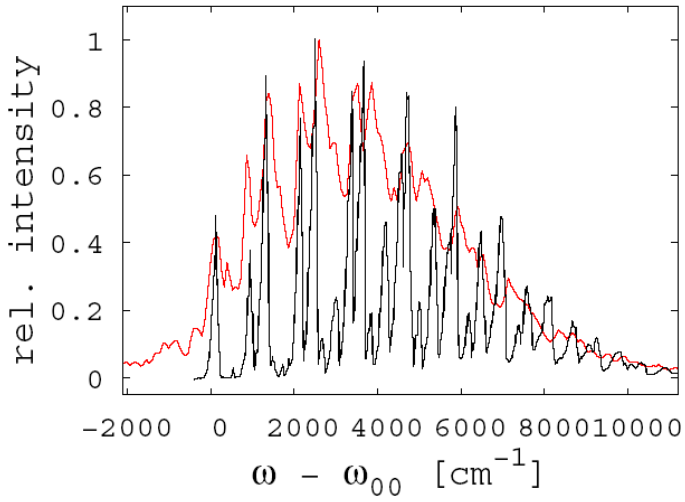

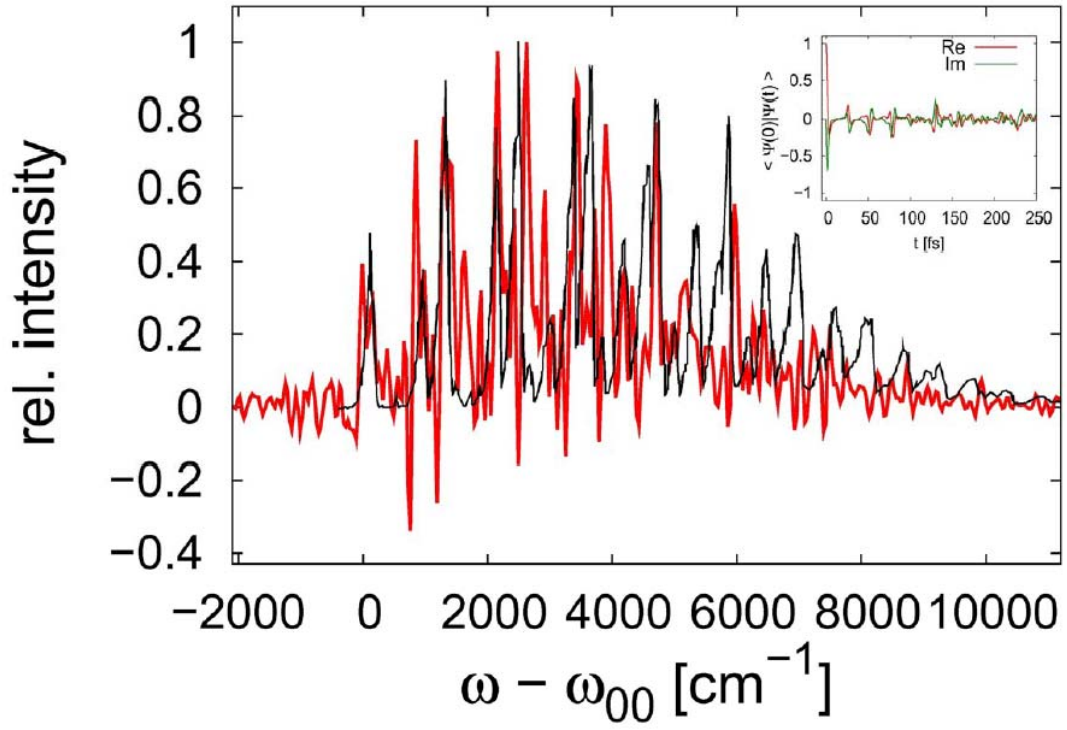

The interaction representation and perturbation theory

Let $\hat{H} = \hat{H}_0 + \hat{H}_1$ and assume that $\hat{K}_0(t) = \exp\left(-\frac{i\hat{H}_0 t}{\hbar}\right)$ is known.

Write down the exact propagator as: $\hat{K}(t) = \exp\left(-\frac{i\hat{H}t}{\hbar}\right) = \hat{K}_I(t)\hat{K}_0(t)$

Then, as is well known

$$i\hbar\frac{\partial \hat{K}_I(t)}{\partial t} = \hat{K}_I(t)\left[\hat{K}_0(t)\hat{H}_1\hat{K}_0(t)^{\dagger}\right] \equiv \hat{K}_I(t)\hat{H}_1(-t), \qquad \hat{K}_I(0) = \hat{I}$$

A semiclassical initial value representation approximation for the interaction propagator may be written as:

$$\hat{K}_{I,0}(t) = \int_{-\infty}^{\infty}\frac{dpdq}{2\pi\hbar}\exp\left[-\frac{i}{\hbar}\int_0^t dt'\,\hat{H}_1(-t')\right]\left|g(p,q)\right\rangle\left\langle g(p,q)\right|$$

$$\hat{K}_{I,0}(t) = \int_{-\infty}^{\infty} \frac{dpdq}{2\pi\hbar} \exp\left[-\frac{i}{\hbar} \int_0^t dt' H_1(p,q;-t') \right] \left| g(p,q) \right\rangle\left\langle g(p,q) \right|$$

Why is this interesting? Consider the overlap function

$$c(t) = \left\langle \Psi \left| \hat{K}(t) \right| \Psi \right\rangle = \left\langle \Psi \left| \hat{K}_I(t) \hat{K}_0(t) \right| \Psi \right\rangle$$

where $\hat{K}_0(t)$ is the numerically exact MCTDH propagator obtained with a semi-empirical potential V_0. Then $\hat{H}_1 \equiv \hat{V} - \hat{V}_0$ is the difference between the first principles force field and the approximate one. $H_1(p,q;-t)$ involves trajectories propagated on the semi-empirical potential only.

Advantages of such a methodology:

- H_1 is small, the integrand is not too oscillatory
- The classical trajectories are generated by the analytical potential,
  a relatively fast and cheap process.
- The first principles force field is sampled with relatively large time steps.
- Derivatives of the first principles force field are not needed.
- It makes full use of the known powerful available quantum dynamics
  methods.

- One may estimate the error:

$$i\hbar\frac{\partial\hat{K}_{I,0}(t)}{\partial t}=\hat{K}_{I,0}(t)\hat{H}_1(-t)+\hat{C}_I(t)$$

$$\hat{C}_I(t)=\int_{-\infty}^{\infty}\frac{dpdq}{2\pi\hbar}\exp\left[-\frac{i}{\hbar}\int_0^t dt'\,H_1(p,q;-t')\right]\left|g(p,q)\right\rangle\left\langle g(p,q)\right|\left[H_1(p,q;-t)-\hat{H}_1(-t)\right]$$

But

$$H_1(q(-t))-\hat{H}_1(-t)\approx H'_1(q(-t))\left[q(-t)-\hat{x}\right]$$

In other words, one may estimate the magnitude of the leading order correction term without need to compute the global force field.

Summary

Quantum dynamics presents a numerical challenge:

a. Beat the exponential scaling with dimensionality

b. Base it on a first principles force field computation

Semiclassics offers some interesting possibilities:

1. Intuitive physical description.
2. Insight into quantum effects such as coherence and tunneling
3. Combination with numerically exact methods possible via perturbation theory
4. Quantum corrections possible through a generalized time dependent perturbation theory

This may be solved as before:

$$\hat{K}_{I,0}(t-t') = \hat{K}_I(t-t') + \frac{1}{i\hbar}\int_{t'}^{t} ds \hat{K}_I(t-s)\hat{C}_I(s)$$

So that $$\hat{K}_{I,1}(t-t') = \frac{i}{\hbar}\int_{t'}^{t} ds \hat{K}_{I,0}(t-s)\hat{C}_I(s)$$

or:

$$c_1(t) = \left\langle \Psi \middle| \hat{K}_{I,1}(t) \middle| \Psi(t;0) \right\rangle = \left\langle \Psi \middle| \frac{i}{\hbar}\int_0^t ds \hat{K}_{I,0}(t-s)\hat{C}_I(s) \middle| \Psi(t;0) \right\rangle$$

$$= \int_{-\infty}^{\infty} \frac{dpdq}{2\pi\hbar} \int_{-\infty}^{\infty} \frac{dp'dq'}{2\pi\hbar} \exp\left(-\frac{i}{\hbar}\left[W_1(p,q;t-s) + W_1(p',q';s) \right] \right)$$

$$\left\langle \Psi \middle| g(p,q) \right\rangle \left\langle g(p,q) \middle| g(p',q') \right\rangle \left\langle g(p',q'), \middle| \left[H_1(p',q';-s) - \hat{H}_1(-s) \right] \Psi(t;0) \right\rangle$$